Journal of Volcanology and Geothermal Research 477 (2026) 108664

Contents lists available at ScienceDirect

Journal of Volcanology and Geothermal Research

journal homepage: www.journals.elsevier.com/journal-of-volcanology-and-geothermal-research

Development and hazard potential of dike-fed eccentric vents during the 2021 Cumbre Vieja eruption, La Palma (Canary Islands)

David Sanz-Mangas [a,e,*], Inés Galindo [a], Agust Gudmundsson [b], Raúl Pérez-López [c], Miguel Ángel Rodríguez-Pascua [d], Rayco Marrero [a], María Ángeles Perucha [d], Juan Carlos García-Davalillo [c], Juana Vegas [d], Nieves Sánchez [a]

[a] CN Instituto Geológico y Minero de España (IGME-CSIC), Canary Unit, Alonso Alvarado, 43, 35003 Las Palmas de Gran Canaria, Spain
[b] Department of Earth Sciences, Royal Holloway University of London, Queen's Building, Egham TW20 0EX, UK
[c] CN Instituto Geológico y Minero de España (IGME-CSIC), La Calera, 1, Tres Cantos, 28760 Madrid, Spain
[d] CN Instituto Geológico y Minero de España (IGME-CSIC), Ríos Rosas, 23, 28003 Madrid, Spain
[e] Universidad Complutense de Madrid, Área de Petrología y Geoquímica; Madrid, Spain

A R T I C L E I N F O

Keywords:
Eruptive fissures
Vent opening
Fissure development
Feeder dike
Volcanic hazards

A B S T R A C T

During the first stage of the Tajogaite 2021 eruption at Cumbre Vieja volcanic ridge on La Palma Island, a scoria cone formed when four major vents merged into one main eruptive fissure. The explosive upper part of the volcanic complex generated columns of gas and ash that reached about 9 km a.s.l. while the effusive lower part produced lava flows covering some 12.4 km^2. At later stages of the eruption, multiple fractures and more than 100 eccentric and distal vents opened at distances up to three kilometres from the main eruptive fissure. The new vents issued degassed pāhoehoe lavas that rapidly invaded previously unaffected urban and agricultural areas. The aligned vents, fissures and fractures strike NW-SE, N-S and ENE-WSW. Spatial and field analyses suggest that the eruption was supplied with magma through two feeder dikes whose location was largely controlled by pre-existing crustal discontinuities and heterogeneities. Feeder-dike induced surface deformation, such as a graben, tectonic fractures of various sizes, and local flank collapses of the scoria cone, occurred during the opening of the vents. Detailed studies of the relationship between tectonic fractures, gas emission, and dike propagation can be used to improve assessment of potential hazards during evolving eruptive dynamics and vent openings in monogenetic volcanoes.

1. Introduction

Volcanic eruptions have a direct impact on society since erupted lavas, fallout deposits, lahars and pyroclastic density currents (PDC) may damage or destroy infrastructures and buildings (Martí et al., 2022; Meredith et al., 2022). In monogenetic volcanic fields, the occurrence of spatially separated volcanic vents during eruptions is common; however, the *syn*-eruptive sudden opening of distal vents far from the main eruptive fissure significantly increases the volcanic hazard. Recent studies indicate the importance of understanding vent opening in fissure eruptions and their strong relationship with pre- and syn-eruptive tectonic controls, particularly since some dikes may use pre-existing fractures for their ascent paths (Galindo and Gudmundsson, 2012; Gudmundsson, 2022; Hjartardóttir et al., 2023; Ducrocq et al., 2024; Sigmundsson et al., 2024).

During large monogenetic eruptions with high-effusive activity, compound lava flows form very complex lava flow fields that can cover tens of square kilometres as well as flow for distances up to tens of kilometres while, commonly, burying crops and causing considerable damage to urban areas (Meredith et al., 2022; Walker, 1971; Jenkins et al., 2017). Also, monogenetic volcanism may be a part of a complex history of the eruptive style and pose varying volcanic hazard conditions due to their frequent occurrence in different volcanotectonic settings, opening fissures that result often in variable eruptive behaviour (Smith and Németh, 2017; Romero et al., 2022; Bonadonna et al., 2022).

In this context, fissure eruptions are common in rift zones, where

* Corresponding author.
E-mail addresses: david.sanz.mangas@ucm.es, d.sanz@igme.es (D. Sanz-Mangas), i.galindo@igme.es (I. Galindo), Agust.Gudmundsson@rhul.ac.uk (A. Gudmundsson), r.perez@igme.es (R. Pérez-López), ma.rodriguez@igme.es (M.Á. Rodríguez-Pascua), r.marrero@igme.es (R. Marrero), ma.perucha@igme.es (M.Á. Perucha), jc.garcia@igme.es (J.C. García-Davalillo), j.vegas@igme.es (J. Vegas), n.sanchez@igme.es (N. Sánchez).

https://doi.org/10.1016/j.jvolgeores.2026.108664
Received 5 April 2026; Received in revised form 3 June 2026; Accepted 5 June 2026
Available online 10 June 2026

dikes propagate from deeper magma reservoirs to shallow magma chambers. These intrusions may either continue their ascent by feeding a dike that reaches the surface and generates a fissure eruption (Galindo and Gudmundsson, 2012; Gudmundsson, 2022), discharging lava flows far from the main vent (Andronico et al., 2005) or become arrested before. Alternatively, some regional dikes, particularly those injected far from central volcanoes, propagate directly from deep-seated reservoirs to the surface (Gudmundsson, 2020). In the Canary Islands (Fig. 1A), most volcanoes are formed from effusive Strombolian basaltic eruptions, with the primary hazard being the effusion of substantial volumes of lava (Romero, 1991; Romero and Beltrán, 2015). In addition, basaltic lava flows possess potential hazard during the first stages of the eruptive

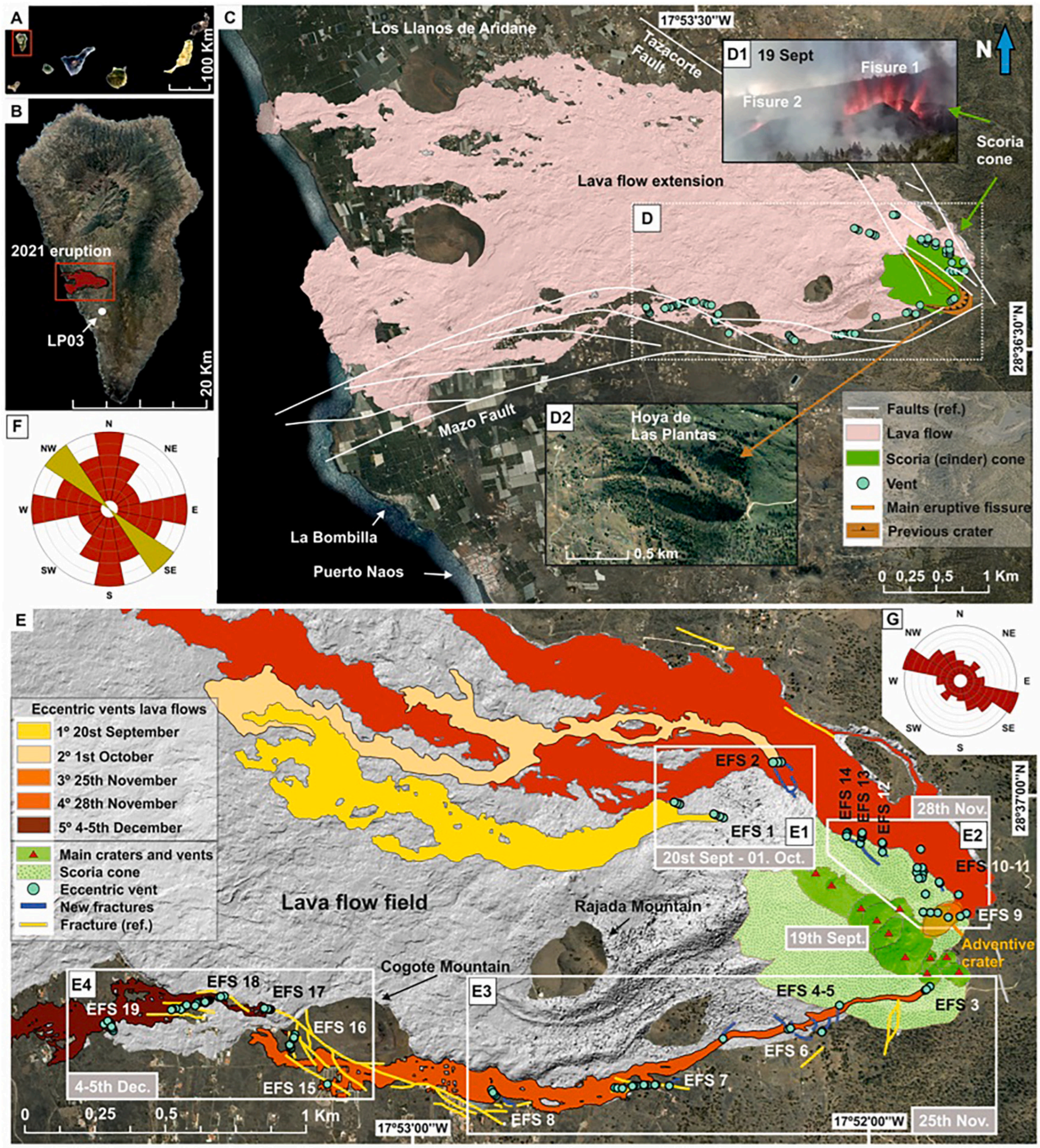

Fig. 1. A) Location of La Palma Island in the Canary archipelago. B) Location of the Tajogaite Volcano, which erupted on 19, September,2021 and the position of GNSS Station LP03. C) Extension of lava flow field and scoria cone (green arrows), main eruptive fissure and the location of eccentric and distal vents. Distribution of the faults described by (Rodríguez-Pascua et al., 2024) in white. Also shown is the location of the localities of La Bombilla, Puerto Naos and Los Llanos de Aridane urban areas. D1) September 19th photograph with the initial scoria cone well-developed with Strombolian activity starting to grow on. D2) Satellite image of the Prehistoric Crater of Hoya de Las Plantas (brown arrow) before the eruption. E) Study zone location with details of the scoria cone, main craters with vents and adventive crater in orange, eccentric and distal vents location grouped in eruptive fissural segments (EFS). Fractures from previous work (Rodríguez-Pascua et al., 2024), new fractures located and lava flows discharged from vents between 20 of September and 5 of December. F) Rose diagram showing the directions of the EFS, vents-alignments in red and the main fissure in yellow. G) Rose diagram of (Rodríguez-Pascua et al., 2024) fractures produced during the event measured in the field and new fractures studied in videos and their estimated strike. EFS numbered in order of aperture, and the inferred dike direction are also shown. The initial eruptive distal vents opened higher up in the scoria cone whereas the subsequent distal vents opened in a lower altitude downhill slope. Most of the vents show two main directions: on the northern side of the scoria cone the strike is NW-SE and on the southern part E-W. Satellite Images and DEM taken from Pléiades1 "© CNES (2021)", Distribution Airbus DS and "TICOM soluciones S.L – GRAFCAN – Gobierno de Canarias" - Accessed 14/09/2025.https://tiles.arcgis.com/tiles/hkQNLKNeDVYBjvFE/arcgis/rest/services/dron_fotogrametria_01102021_csic/MapServer (For interpretation of the references to colour in this figure legend, the reader is referred to the web version of this article.)

fissure-opening due to its high discharge rate, low viscosity and rapid flow that allows the lava to spread quickly (Meredith et al., 2022; Calvari, 2019). Thus, being one of the main impact on communities, completely destroying buildings and infrastructure as in recent eruptions: Nyiragongo 2021 (3600 buildings, Congo) or Kilauea in 2018 (700 buildings, Hawaii, EEUU) (Meredith et al., 2022).

The lack of detailed knowledge of long-term eruptive history of the Canary archipelago makes accurate estimates of volcanic hazards difficult. This is particularly notably due to the large increase in populated urban areas, especially in the past 50 years. For comparison, the total population was around 160 thousand in the 18th century but reached over 2.2 million in the early part of the 21st century (Instituto Canario de Estadística - ISTAC 2020 – (Meredith et al., 2022)).

There are 15 historical eruptions recorded in the Canary Islands, some of which resulted in substantial damage to infrastructures and buildings, as well as deaths, such as the Garachico eruption in Tenerife in 1706 CE and the Timanfaya eruption in Lanzarote in 1730–1736 CE (Romero, 1991; Longpré and Felpeto, 2021). The most recent monogenetic eruption is the one we focus on, the 2021 Tajogaite eruption at the Cumbre Vieja Volcanic Ridge (henceforth CVR) on the island of La Palma (Fig. 1B and C). The CVR, a large volcanic structure with a main axis trending N-S, has been active for over 123 ka (Carracedo et al., 2001). The CVR has the highest eruption frequency in the Canary Islands, a total of eight fissure-type and monogenetic eruptions since the 15th century (Carracedo et al., 2001). Prior to the Tajogaite eruption, which began on 19 September 2021, La Palma was in an alert state (from 11 September) because of an intensification of seismic activity. Seven days before the eruption, the Canary Islands Special Plan for Volcanic Emergencies of the Government of the Canary Islands (PEVOLCA (PEVOLCA Scientific Committee Reports, 2021)) was activated.

The Tajogaite volcanic process in the CVR began with the injection of a shallow magma intrusion (Montesinos et al., 2023) part of which eventually reached the surface through a feeder dike at two elongated vents which were separated laterally by 200 m along a line trending NW-SE (Fig. 1D and D1) and located in an older Holocene volcano ("Hoya de las Plantas") (Fig. 1 D2). Eventually, these vents merged into one main eruptive fissure that formed a scoria (cinder) cone (Fig. 1 D1) (PEVOLCA report 19/09/2021 20:30 h. (PEVOLCA Scientific Committee Reports, 2021; Birnbaum et al., 2023)). The eruption was fed by two dikes emplaced with different attitudes, one very shallow in the crust (0.9 km) and one deeper (1.4 km) (De Luca et al., 2022a; Walter et al., 2023).

The eruption lasted 85 days and 8 h and had a Volcanic Explosivity Index (VEI) of 3, showing explosive Strombolian behaviour (25 and references therein). The erupted lava flows impacted more than 1240 ha of urban area and agricultural land, including the destruction of 2988 buildings and additionally damaging 138 (Fig. 1C) and one fatality due inhalation of toxic gases (Copernicus Emergency Management Service. https://mapping.emergency.copernicus.eu/activations/EMSR546/; [Benito et al., 2023]). Lava flows showed two main lithological types: a first amphibole-pyroxene bearing tephrite during the first stages of eruption, followed by an olivine-pyroxene bearing basanite till the end of it (Sanz-Mangas et al., 2024a). Tephrite lavas were thicker 'a'ā and blocky types that formed broad channels and the later lavas were a more fluid pāhoehoe type that marked the later stages of the eruption [25; 27].

During and after the eruption, diffuse gas emissions of CO_2 have also affected the coastal areas of La Bombilla and Puerto Naos (Fig. 1C for location) (PEVOLCA 22/04/2022 (PEVOLCA Scientific Committee Reports, 2021)) over 5 km from the main eruptive fissure. Gas emissions persisted for a period of four years, preventing residents from returning to the affected areas (Viveiros and Silva, 2024). CO_2 was also studied in the groundwater where the greatest increase occurred after the eruption (Jiménez et al., 2024) and coincided with the gas emission on the surface.

During the 2021 eruption, several new distal eruptive vents opened up as far as 3 km from the main vent (Fig. 1D and E, map with all the eruptive fissures/vents located and coded by date of opening) following different alignments (Fig. 1F, (Calvari et al., 2026; González, 2022; Sanz-Mangas et al., 2024b)) with large volumes of lava flowing into urban areas. These distal vents were associated with small cracks, fractures and larger fissures, trending NW-SE and E-W, parallel to two main faults (Fig. 1C, E and G, (Rodríguez-Pascua et al., 2024; Rodríguez-Pascua et al., 2026)). Despite the importance of these distal vents, which emitted five indistinct lava flows during the eruption (Fig. 1E), their location and origin have received little attention. A review of historical eruptions in La Palma (p.e., Jedey in 1585, San Martín de Tigalate in 1646, El Charco in 1712, and San Juan eruption in 1949) suggests that, during eruptions, several eruptive fissures may extend many kilometres from the main volcanic cone or vent (Romero, 1991; Longpré and Felpeto, 2021) (Fig. 2). The study of vent alignment in eruptions is crucial for tracing the development of multi-vent eruptions, thereby providing a more reliable basis for hazard assessment in future eruptions in populated areas (Becerril et al., 2013). The vent/fissure arrangement also provides information on the local stress field since their formation is due to dike segments reaching the surface, and these segments, in turn, are largely controlled by the local stress field and, partly, existing discontinuities in the crust (Gudmundsson, 2022; Gudmundsson, 2020; Montesinos et al., 2023). The presence of two distinct magmas ascending and secondary paths was confirmed by (Ubide et al., 2023; Zanon et al., 2024), suggesting that two feeder dikes (or a multiple dike) supplied magma during the eruption.

The main aim of this study is a characterisation of the volcanic vents, eruptive fissures, dike-induced fractures formed during the 2021 Tajogaite eruption in CVR, and emitted lava flows. The focus is on analysing the sequence of events of the opening and the spatial distribution and directions of the volcanic fissures, the dike-induced surface fracturing, and how these can be used to infer the feeder-dike propagation close to the surface. Additionally, we discuss the implications of the main results

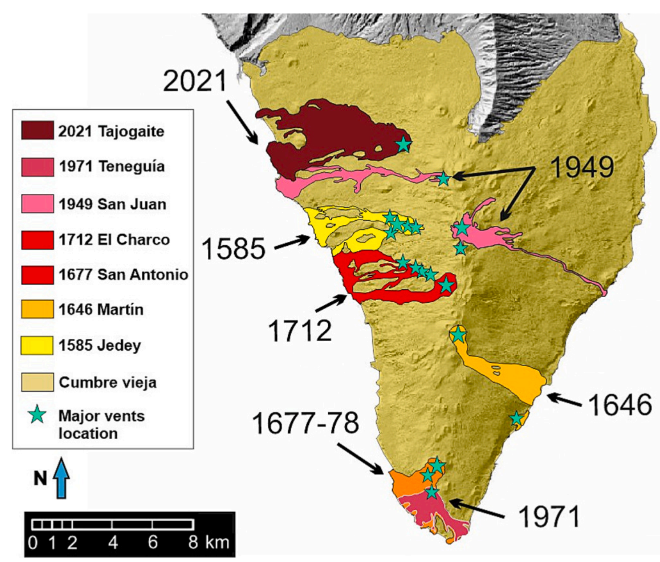

Fig. 2. Historical eruptions (<500 years) and lava flows cover in red of CV volcanic rift and approximately midpoint of the main vents marked with a big blue star and smaller start for distal vents (adapted from MAGNA, GEODE ((https://mapas.igme.es/gis/rest/services/Cartografia_Geologica/IGME_Geode_50/MapServer)). 1585 Jedey eruption, 1646 Martí-Tigalate, 1677–78 San Antonio-Fuencaliente, 1712 El Charco, 1949 San Juan eruption in red shapes and last 1971–2021 from Teneguía and Tajogaite eruptions in black and garnet shapes respectively. DEM from Pléiades1 "© CNES (2021)", data provided by Distribution Airbus DS and "TICOM soluciones S.L – GRAFCAN – Gobierno de Canarias"- Accessed 12/12/2024. https://catalogo.idecanarias.es/geonetwork/srv/spa/catalog.search#/metadata/spagrafcan_136MDS5m2010_20160101 (For interpretation of the references to colour in this figure legend, the reader is referred to the web version of this article.)

for related hazards, including the lava emplacement, the stability of the scoria cones, and the diffuse gas emission.

Our results suggest that the dynamics of Strombolian eruptions may go beyond the simple formation of a monogenetic cone, revealing a complex plumbing system influenced by feeder-dike interactions with pre-existing fractures and the active stress field. The 2021 Tajogaite eruption presents an excellent opportunity to study these dynamics, as multiple distal and eccentric vents formed during the eruption. Our analysis indicates the presence of a complex feeding system, which was also influenced by existing discontinuities, that allows magma to propagate from the main fissure to far-away areas opening unexpected distal vents. These vents, distributed over a two-kilometre stretch, impacted multiple urban areas, severely damaging infrastructures. The opening of distal vents far from the main fissure pose a major hazard of fissure eruptions and determine the possible impact, reinforcing the need for understanding volcano-tectonic structures in volcanic zones, since they control the superficial movement of magma.

2. Geological background – Historical eruptions and vents from CVR

CVR complex has 1949 m high and ~ 20 km-long is predominantly composed by basaltic lavas and pyroclasts (19). The eruptions that characterize the formation CVR are fissure-type basaltic with minor phonolitic intrusions. Previous studies of historical eruptions on La Palma (Martí et al., 2022; Romero, 1991; Longpré and Felpeto, 2021; Carracedo and Troll, 2016) suggest that most of the events developed distal vents far from the main vent. Examples include the Jedey eruption in 1585 CE, Martín in 1646 CE, San Antonio in 1677–1978 CE, El Charco in 1712 CE and San Juan in 1949 CE (Fig. 2).

Historical chronicles on the 1585 CE Jedey eruption are scarce (Fig. 2). Apparently, the eruption had three principal vents that opened in the western flanks of the CVR as a part of a 1500 m long and WNW-ES*E*-striking fissure (Romero, 1991; Longpré and Felpeto, 2021; Hernandez-Pacheco and Valls, 1982). Some tectonic fractures also opened at the eruption site. The eruption was characterised by the extrusion of high-viscosity domes of phonolitic composition. The upper vents had explosive activity and formed a scoria cone. The effusive activity was focused at the southern base at a lower altitude opening through eccentric vents, the lavas issued being of basanite-tephrite composition.

The 1646 CE Martín (or Tigalate) eruption (Fig. 2) had two main vents. The eruption, however, started with several vents in the central part of the CVR, but these ended up merging into one large fissure. This fissure was 1275 m long, striking N-S. The fissure had two minor segments that propagated to the south during the first days of the eruption. All eruptive materials were basanitic. The upper vents initially had an explosive behaviour but gradually became more effusive. A second distal double-vent opened after several days some 4 km to the east of the first main eruptive fissure, at the coast, and had dominantly effusive activity. This distal vent was characterised by a Hawaiian-style eruption and spattering through multiple hornitos (Romero, 1991; Longpré and Felpeto, 2021) and striking NW-SE.

Between 1677 and 1678, the San Antonio (or Fuencaliente) eruption took place. At least three vents opened and issued basanitic lavas (Fig. 2). The eruption had a main vent in the mid-southern part of the CVR ridge and several additional vents at lower topographical levels, striking E-W and NW-SE. The alignment defined a 900 m-long fissure (Longpré and Felpeto, 2021). The lower vents were effusive and the upper vent had and explosive activity.

El Charco eruption of 1712 occurred in the main central part of CVR on its western flank (Fig. 2). The eruption developed three major vents with a total lineament (fissure) length of 2500 m. The upper vent formed an N-S elongated (striking) scoria cone with considerable explosive activity. The feeder-dike subsequently propagated N*E*-SW resulting in the opening of the two additional and mainly effusive vents at lower topographic levels. Close to the end of the eruption the last vent opened, effusive and striking NW-SE (Romero, 1991). More specifically, its activity was Strombolian and Hawaiian with hornitos and spatter of basanite to tephrite composition.

One of the previous eruptions developing vent-opening at considerable distances before the present one was the 1949 San Juan eruption. As in previous eruptions, the vents started in the mid-zone of the CVR and propagated first to the south, striking N-S, and later to the NW (Fig. 2). The lava, mainly basanites and tephrites, flowed down both flanks of the CVR. Associated with the 1949 eruption, several faults, fractures and cracks were found on the surface, probably due to the shallow dike emplacement (Klügel et al., 1999). However, other authors (Day et al., 2000) suggested a fault system formed in the western side of CVR that controlled the multi-vent development of the 1949 eruption. The three main vents that formed during the eruption were separated by a maximum distance of 3500 m. The first vent, named Duraznero, showed mainly explosive activity with strong phreatomagmatic pulses. Few days later, the second vent opened, named Llano del Blanco. This vent was mainly effusive, producing fast-flowing (some reaching 10 m/s) pāhoehoe lava flows with associated lava tubes (Klügel et al., 1999). The third vent, named Hoyo Negro, produced pāhoehoe lava through fissures with E-W orientation (Romero, 1991).

3. Methods

In this work, several approaches were applied to enhance understanding of the multi-vent opening process over the entire 85-day eruption period and to generate a chronological interpretation in 24-h format. Remotely Piloted Aircrafts (RPAs) from the IGME-CSIC Aerial Work Service (STA), fieldwork and Geographic Information Systems (GIS) were used to monitor the entire eruption. This activity formed part of IGMEs continuously observation of the lava-flow field evolution for daily statements as to the emergency based on lava-flood invasion forecasting, lava tubes formation and new vents-opening (https://info.igme.es/eventos/Erupcion-volcanica-la-palma/). In addition, we used photogrammetric imagery from the Cabildo de La Palma government (TICOM Soluciones S.L., https://www.opendatalapalma.es/).

Volcanotectonic features were located and measured in the field with GPS and compass, and later mapped and measured with the ©ArcGIS software. The vents described in this study are the emission points at the Earth's surface that discharge volcanogenic material directly. Table 1 supp. With of definitions has been provided in Supplementary Material (Fig. Supp. 1). In the case of vents buried by lava flows during the eruption, the location was inferred using geographical references. We discern between new vents and lava tube-drainages based on the related gas emission, since the first were related to episodic HCl-CO_2 diffuse emission and radon (Rn) emission. The gases were measured with Industrial Scientific monitor multi-gas VENTIS IBRID-MX6 equipped with pump, VENTIS Pro5 and Blackline Safety G7C Multi-Gas, measuring punctual CO, CO_2, H_2S, SO_2 (in ppm) and O_2 (in % Vol). Also, a portable Alfa spectrometer SARAD model RTM2200 was used for Rn and CO_2 measurements. Some of the vents associated with fractures also showed thermal anomalies between 60 and 80 °C. After the eruption, these vents and fractures became sites of H2O vapour emission and the remains of dead plants and small animals. Temperature was measured with Type-K thermocouple of 1 m-length and 6 mm-width connected to a TENMA 72–7715 thermometer.

The vents were marked with a point at the location spot with fountaining activity, spattering or bubble bursting when the vents were covered with lavas, or, when available, through RPAs videos. When the lava was issued from a fissure-type vent, the point marks the central part of the lineal structure (usually with lengths <5 m). Alignments of the vents were interpreted as fissures and the surface expression of feeder dikes, on the field usually associated with rough, spiny surfaces of pāhoehoe-type lava flows, abundant spatter deposits, and sometimes hornitos and spatter cones. On ArcGIS, vents aligned were grouped in

Table 1
Main parameters of the eruptive vents (First Stage Vents: FSV, Second Stage Vents: SSV, Third Stage Vents: TSV).

Phase		Date	Distance from Main Fissure (m)	Max. fissure length (m)	Crack number	Mean opening (cm)	Lava speed ($m \cdot s^{-1}$)	Lava flow length (Km)	Lava flow area (ha)	Viscosity (Pa·s)
1	Initial Stage	19/09/2021	–	900	–	–	0.02–0.3	Reference (Calvari et al., 2026)	103	8.1×10^3 to 3.2×10^4
2	FSV 1	20/09/2021	843–998	30–20	–	–	0.5–1	1.8	26.8	389 to 1.2×10^3
3	FSV 2	01/10/2021	846	30	43	–	0.4–2.2 - 2.7	2.3	20.8	144–225 to 6×10^3
4	SSV	25/11/2021	321–761 1013–1192 1602	190 24	49	20	5	1.2	14	78 to 486
5	TSV	28/11/2021	163–464	160	36	50	1–2	4.8	138.2	194–608 to 6.8×10^4
6	SSV 1	04/12/2021	2180 2310 2365 2524–2718	60 40 193	533	20 30 40	0.14–1.7 - 3.1	2.7	31.6	70–202 to 806–9.7×10^3
	SSV 2	05/12/2021	2944	60		–				

fissures, identified with a line between vents located less than 60 m apart and collinear for the study of the orientation of the multivent-opening process. Furthermore, vents and fissures opened with the same conditions (bursting at the same time and proximity) were grouped in eruptive fissural segments (EFS) and numbered in chronological order of vent-opening. The geometrical attributes of the discharged lava flows were obtained from a DEM of 25-m resolution (WGS84 UTM Zone 28 N, Spanish Geographical Institute IGN - www.ign.es -) and photogrammetric flights from Cabildo de La Palma government (TICOM Soluciones S.L., https://www.opendatalapalma.es/) and STA-IGME.

RPA videos and direct measurements also permitted the characterisation of the lava rheology applying Jeffrey's equation for viscosity that provides an effective viscosity using morphological values, mean values of lava thickness and velocity (Jeffreys, 1925; Chevrel and Harris, 2025; Lerner et al., 2024):

$$V = \rho \, g \sin(\alpha) \, d^2 / n \, \eta$$

Being (V) the lava flow velocity measured, (ρ) the lava density, (g) acceleration due to gravity, (α) the slope and (η) the viscosity. (n) is a factor used for wide lava channels with the value of 3 (Booth et al., 1973). The equation used is based on observations during the lava-flow emissions associated to the eccentric vents during the eruption with an apparent very-low viscosity, being similar in behaviour to a Newtonian fluid near the vents, and inferring that the velocity increases proportionally to the square of the lava flow thickness (Moore, 1987). Hence, for very fast-moving lava flows a Newtonian behaviour is assumed, with 2700 $kg \cdot m^{-3}$ for average dense rock value of lava. This value of density is assumed based on mean density between 2600 and 2800 $kg \cdot m^{-3}$ for a typical value of lavas of basaltic composition from La Palma eruptive activity (Ubide et al., 2023; Klügel et al., 1997; Castro and Feisel, 2022). For the central lava flows and channels, the relative velocity of the flowing lava was determined from pieces of cooler crust moving a given distance per unit time (Chevrel and Harris, 2025; Harris et al., 2007). The thickness of the lava flow emitted from the eccentric vents studied in the field rarely exceeds 0.4 m in the proximal zones (<30 m), 0.5 m in the intermediate (<500 m) and up to 1 m in distal zones (>500 m); therefore, these ranges have been used as reference for the viscosity calculation.

The Military Emergency Unit (Henceforth UME) supplied crucial and timely diffuse gas-measurements in their reports. We also used geodetic data from the Spanish National Geographic Institute (IGN) Jedey GNSS Station LP03 (Fig. 1B) (https://www.ign.es/web/gds-gnss-datos-rinex) for interpretations and the PEVOLCA official daily bulletins (https://www.gobiernodecanarias.org/infovolcanlapalma/pevolca/ (PEVOLCA Scientific Committee Reports, 2021)). ©CorelDraw X8 software was used to compose the figures.

4. Dynamics of the Tajogaite multi-vent opening processes

4.1. Chronology of the events

The Tajogaite eruption had a main eruptive fissure where the activity was concentrated, forming the main volcanic cone. However, other eruptive vents opened during the eruption. We describe here the different phases of vent opening, starting with the formation of the main eruptive fissure and following with the eccentric vents episodes. The location of the eccentric vents and the erupted lavas for each episode are shown in Fig. 1E and on Table 1 are the main parameters of the observations.

4.1.1. Phase 1: 19 September-13 December 2021

The eruption began on 19 September 2021, when magma reached the surface at 15:12 h (local time WET) at the location 28°36′58.6" N - 17°52′0.6" W (Fig. 3A), within the "Hoya de las Plantas" Holocene crater (Fig. 1 D2) on steep slopes between 17 and 26 degrees. It formed a *fissure-type vent* (V1) striking NW-SE (azimuth 127°) (Fig. 1F). About fourteen minutes later (15:26 h), a *second fissure-type vent* opened at 220 m from the first vent followed almost immediately by a *third vent* continuing the activity to the NW (V2 and V3, Fig. 3B and C). V2 and V3 merged at 15:28 with V2 in a larger eruptive fissure (Fig. 3D). Also, a scoria cone was already built at V1. After about twenty minutes, a fourth and fifth fissure (V4 to V5) with several vents opened at the SE end of the alignment (Fig. 3E). V5 reached the surface 260 m from V1 at a higher elevation and generated the greatest explosive activity (with little or no flowing lava) of the vent-forming sequence, resulting in several vents emitting ash and gas columns rising to a height of 1500 m above the ground (PEVOLCA report 20:30 h 19/09/2021 (PEVOLCA Scientific Committee Reports, 2021)). V4 and V5 mainly issued water vapour and minor ash. The sixth and final fissure (V6) formed in close proximity to V2 and V3, in the lowest topographic sector located in the northwest

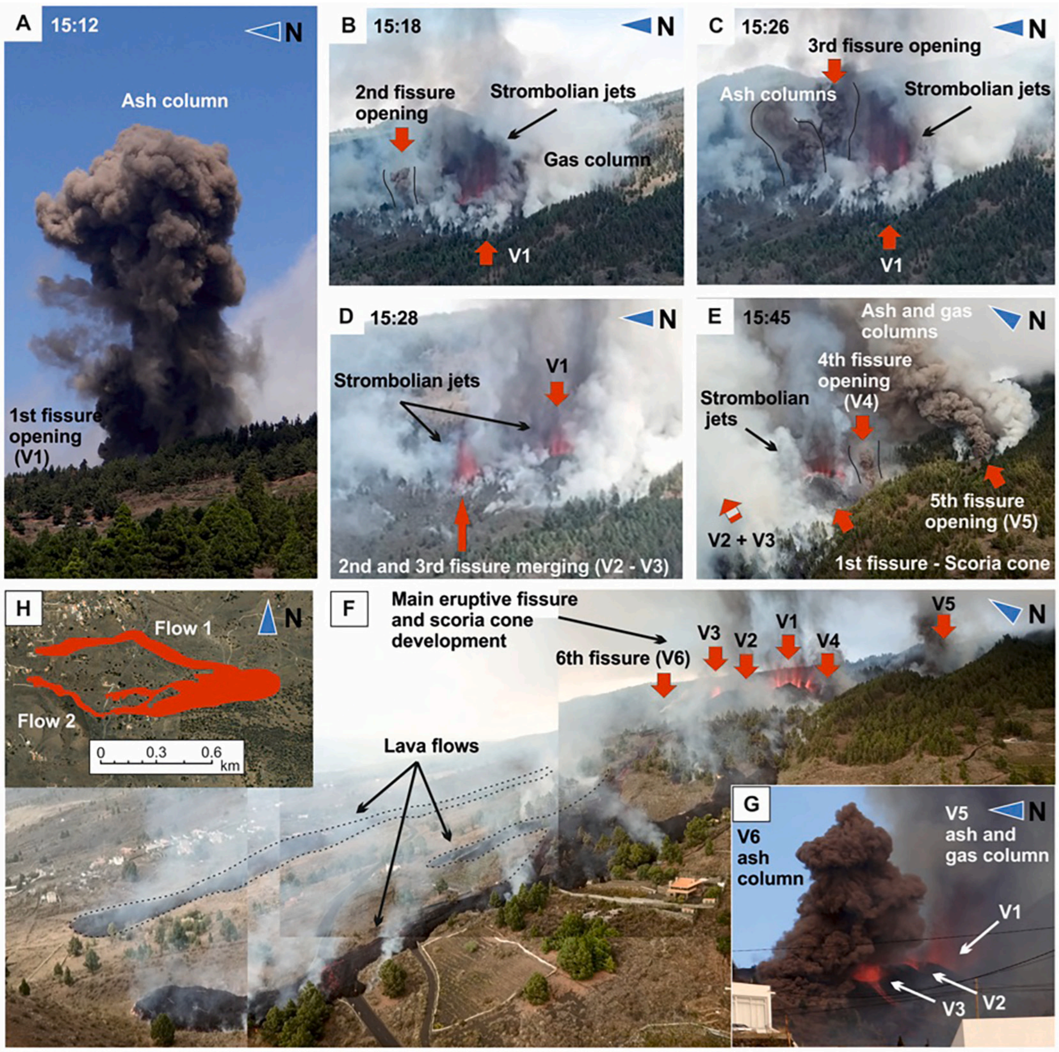

Fig. 3. 19th September field photographs of the first minutes of eruption (pine trees for scale, up to 25 m): A) First fissure-type vent (V1) explosive opening with emission of an ash column reaching an altitude of 1.5 km (PEVOLCA Scientific Committee Reports, 2021); B) V1 propagation with several Strombolian jets formed and second fissure (V2) opening with an initial small ash-column. Note the high amount of gas emission from the prehistoric "Hoya de Las Plantas" rim crater. C) Third fissure (V3) opening between V1 and V2, all of them with Strombolian activity. D) V1-V3 already opened with Strombolian explosive style. The lower vents merge and the effusive activity start emitting 'a'ā lava-flows. E) Fourth fissure opening (V4) at a topographically higher elevation than V1 with explosive style emitting only ash and km-length columns of ash and gases. F) 16:37 composite image from drone images with the total view of the vents that form the main eruptive fissure and opening of fissure V6 with a minor material column, the scoria cone with multiple vents and lava flows emitted. G) Photo of V6 from NW showing paroxysm. H) Main lava flows emitted perimeter during the first stages of the eruption with 18 ha of surface covered. This was a fissure eruption with a progressive alignment of several vents that had a style-development from explosive to effusive within minutes.

(Fig. 3F) with explosive activity (Fig. 3G). Progressively, the effusive activity was concentrated on the lower vents V1, V2 and V3. V6 became inactive, and, during the eruption, the upper vent V5 showed mainly explosive activity with a violent Strombolian behaviour and episodic paroxysms with shock waves and phreatomagmatic pulses with a maximum column height reaching 7700 m a.s.l. (PEVOLCA report 25/12/2021 (PEVOLCA Scientific Committee Reports, 2021)). In this first episode, two main lava flows were flowing to the west, into the Aridane Valley, covering 18 ha (Fig. 3H). The lava flows were mainly 'a'ā-type, between 1.5 and 2 m thick, with initial relative speeds of 0.3 $m \cdot s^{-1}$ (998 $m \cdot h^{-1}$) and reached 700 m-length in less than one hour (Fig. 3F). Afterwards, the lava flow fronts velocity was reduced significantly up to 82 $m \cdot h^{-1}$, not far from the ones measured from the speed measured by previous works (Calvari et al., 2026) with 50 $m \cdot h^{-1}$. Using a constant effusive rate for Jeffrey's equations and the parameters described above, combined with the sharp slope (<26°) and the average rock density of 2700 $kg \cdot m^{-3}$ (described in more detail in the Methods section), the relative viscosity measured from lava flows ranges from 8.1×10^3 to 3.2×10^4 Pa·s. On 20 September, the lava flows extended up to ~3,3 km long and covered 103 ha of surface.

The final "scoria cone complex" termed Tajogaite cone was a single fissure-fed, monogenetic volcanic edifice of > 180 m-high and ~900 m in diameter. Geologically, it consists of a multi-vent eruptive system aligned NW-SE, with explosive and effusive vents. From a petrological point of view, it is subjected by juvenile basaltic–basanitic to tephritic scoria, lava flows, and associated pyroclastic deposits. As a geomorphological element, it forms a composite scoria cone with several craters.

4.1.2. Phase 2: 20–26 September 2021

On 20 of *September*, less than 48 h after the beginning of the eruption and following a surface inflation of 20 cm from the previous day (PEVOLCA report 20/09/2021 (PEVOLCA Scientific Committee Reports, 2021), new vents with effusive activity and spattering were spotted at 22:00 emitting large volumes of pāhoehoe-type lavas through a NW-SE–striking eruptive fissure segment (EFS1) to the NW of the scoria cone (Fig. 1 E1). During this phase two eruptive fissures formed. The first, a 30-m-long NW-striking fissure with four vents, formed approximately 843 m from the main vent (Fig. 4A). Subsequently, a second fissure, located ~998 m from the main vent and with a length of 20 m, was opened showing another three vents (Fig. 4B). The lava flow reached 1.8 km in length, and an estimated 26.8 ha in area, which was covered by later lava flows and pyroclastic fallout. Lava flows evolved, forming short-lived lava tubes during the next day, and formed spatter cones observed in the field (Fig. 4C). Lava flow velocities measured on the night of 20 September ranged from 1 m·s-1 (<30 m from the vents) to 0.5 m·s-1 (<100 m). Using the empirical equation from methods section which allows lava viscosity to be inferred from the lava flows from 20 of September parameters, a value of viscosity between 389 and 1.2×10^3 Pa·s has been estimated. On 23 September, lava was still

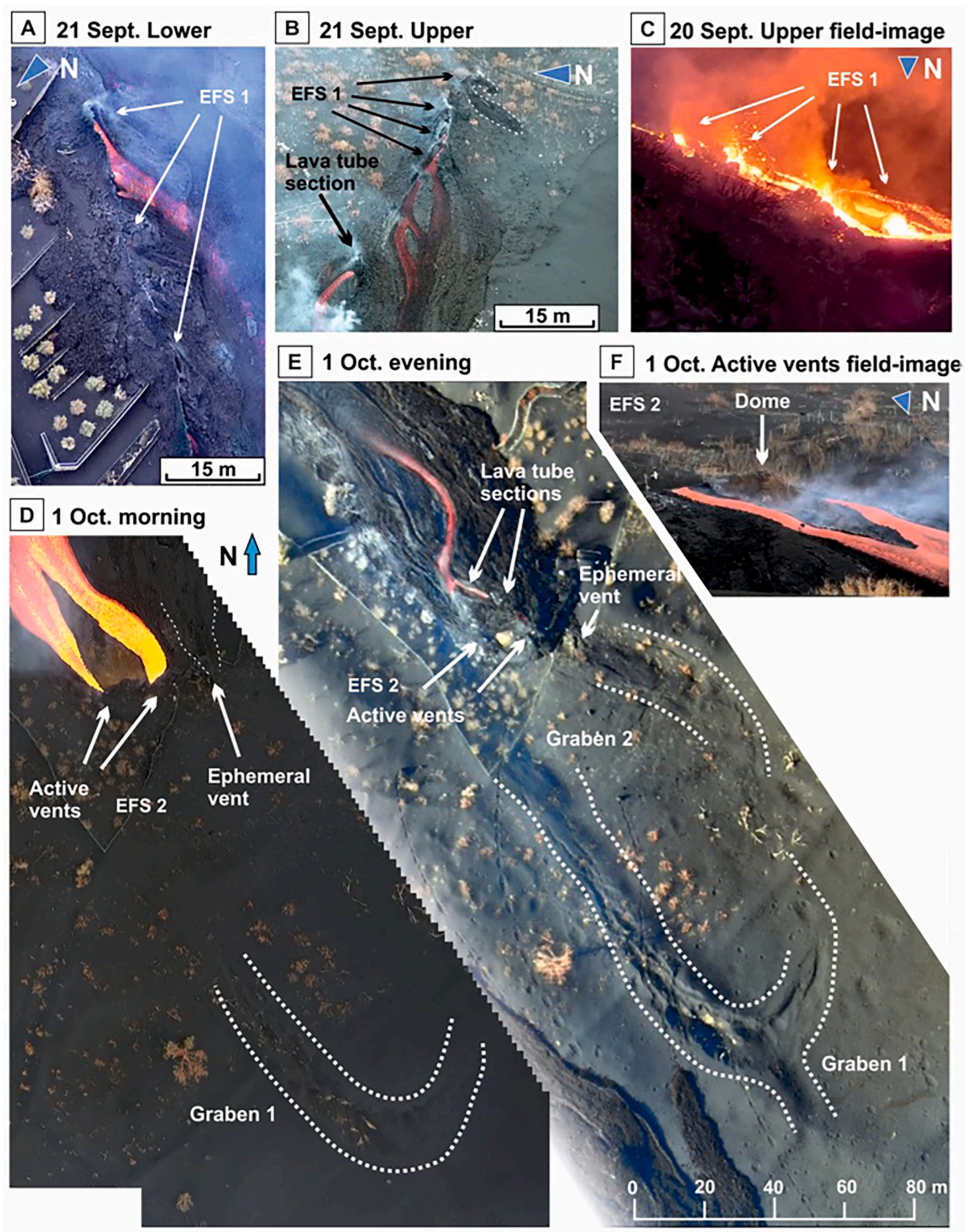

Fig. 4. The first sequence of fissure-type vents began to open on 20 September near the main vent and subsequently propagated towards the WNW. A) lower part of EFS 1 with two observable distal NW-striking vents, lava flows with pāhoehoe morphology that transform quickly to ʻaʻā; B) Upper part of EFS 1 (NW-SE oriented) with at least four vents discharging lava. Second sequence of distal-vents-opening on October 1st: C) 20 September fieldwork image from EFS 1 first insights with the four vents and spatter cones developed. D) RPA images of NW distal eruptive vents of 1 October. RPA photograph of graben 1 spotted early in the morning with a double-distal vent *E*-W oriented (EFS 2) of pāhoehoe-type lava. E) RPA photogrammetric image taken in the evening with graben 1 propagated and graben 2 with lava flow being channelled. F) Field image showing the detail of EFS vents emitting low-viscosity degassed pāhoehoe lava. Early lavas start very fluid with a Hawaiian effusive style. Note that the lava tube development within hours. The tectonic graben-like structure is ephemeral in the first stages and evolves into a deeper and longest morphology probably related to the deflation due to the loss of pressure of the injected dike. Photogrammetry image taken from Cabildo Insular de La Palma and CSIC – Accessed 12/12/2024.

observed through these distal vents, but on 24 September, activity ceased. On 27 September, the eruption paused for approximately 10 h (Ubide et al., 2023), with no seismic activity, shock waves, or emissions of lava flows, ash, or ballistic blocks. It then resumed in a moderate state, gradually intensifying overnight until it regained its previous dynamic.

4.1.3. Phase 3: 1–3 October 2021

On 1 *October*, after an intense fumarolic activity in the northern part of the scoria cone, a new episode started ~846 m from the main eruptive fissure (EFS 2, Fig. 1 E1). In the early morning, at 02:30 h, three vents opened in slopes dipping up to 26° along a fissure with an E-W alignment and displaying effusive activity. These vents displayed a 40 m-wide horseshoe-shaped graben morphology north of the scoria cone (Fig. 4D), containing a total of 43 cracks and with a length of ~700 m. The graben propagated to the NW for up to 120 m during the day and became deeper as the eruption progressed. One of the vents was very ephemeral and became inactive early (Fig. 4D and E), while the others were active for three days, with an effusive activity of degassed fast-flowing thin

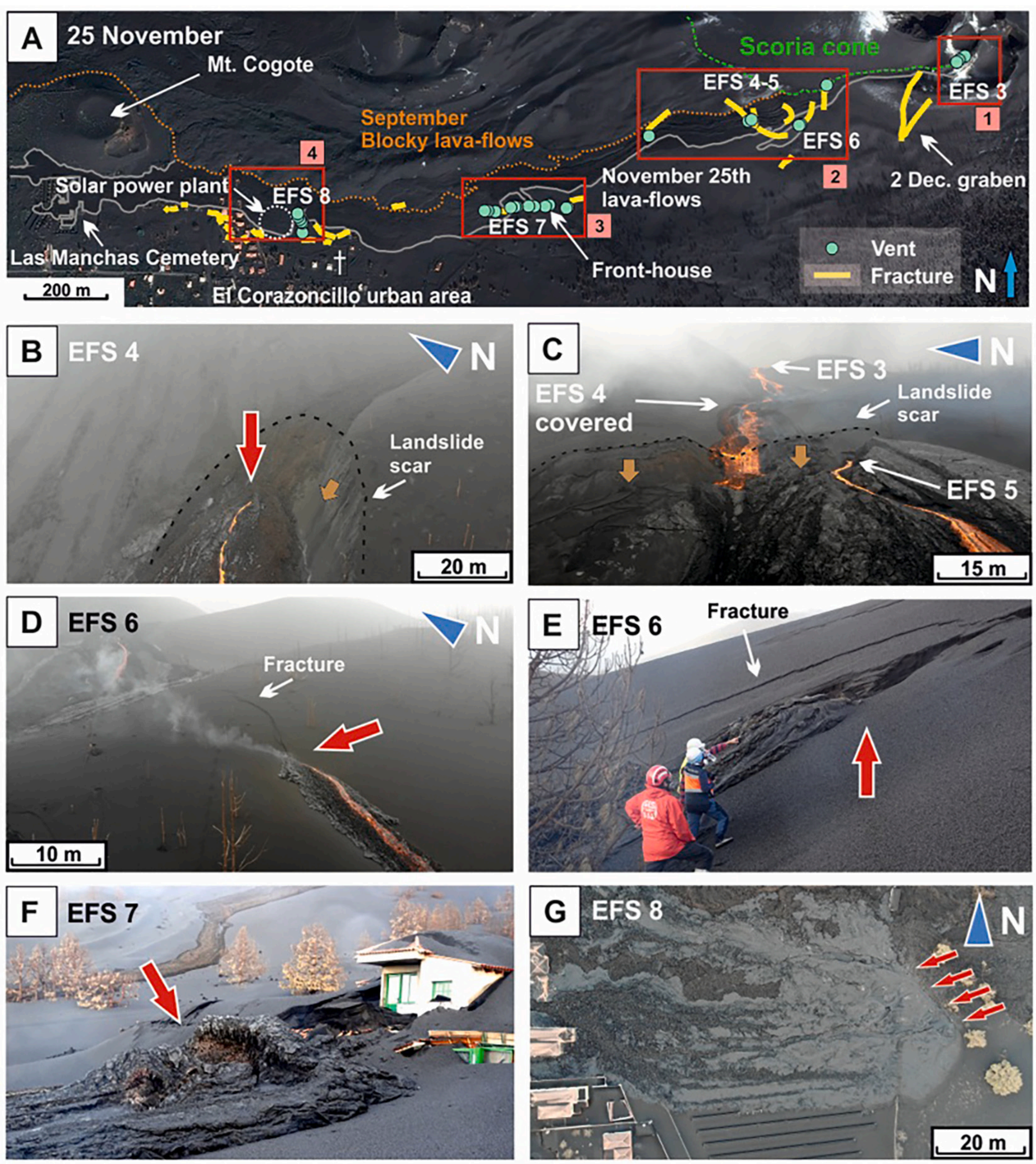

Fig. 5. A) Distal vents locations, numbered according to distance from the main vent and dates: region SE of scoria cone with graben formed on 2 December: 1 (EFS 3, phreatomagmatic crater-border) & 2 (EFS 4–6, scoria cone slope): 24–25 November morning. Region at El Corazoncillo urban area: 3 (EFS 7, front-house): 25 November evening; 4 (EFS 8, solar power plant). The orange dotted line represents blocky lava flow contact from September, grey line shows lava flows from 25 November. Dagger marks the proximal location of the death confirmed. RPAs drone field-photographs taken during La Palma eruption: B) early images from 25 November with EFS 4 vent opening at the southern flank of the scoria cone; C) later image of the south-western base cone with EFS 3 to 5 with landslide scar of the slope failure; D) EFS 6 striking SW with vent that burst up from a listric fault (NNW fault scarp marked in dashed line and brown arrow marking the direction of the landslide 1). Fieldwork images of the vents after the event: E) EFS 6 with detail of the fissure with lava emitted and fracture; F) EFS 7 with vents from the 25 November late-evening, the sequence cross beneath a house forming a small spatter cone. G) RPA image of EFS 8 with pāhoehoe lava emitted after EFS 7. Red arrows mark the vent's location. Note that the propagation of vents to the WSW opened following 3 main directions: NW-SE, E-W and ENE-WSW, these distal fissure-type vents were related with the opening of fractures in the terrain and houses following the same directions and emitting very fast-pāhoehoe lava-type. Photogrammetry images taken from Pléiades1 "© CNES (2021)", data provided by Distribution Airbus DS and "TICOM soluciones S.L – GRAFCAN – Gobierno de Canarias"- Accessed 12/12/2024. https://tiles.arcgis.com/tiles/hkQNLKNeDVYBjvFE/arcgis/rest/services/dron_fotogrametria_01102021_csic/MapServer (For interpretation of the references to colour in this figure legend, the reader is referred to the web version of this article.)

pāhoehoe lava flows advancing at ~2.7 m·s^{-1} next to the vents to ~2.2 m·s^{-1} in the proximal area (<30 m from the vents) (Fig. 4F) and then to around 0.4 m·s^{-1} in the distal zones (>300 m from the vents, the lava being 1 m thick) where the lavas changed into slowly moving ‘a'ā-types. Taking the previous data into account, viscosity ranged from 144 to 225 Pa·s in the proximal zone of the vent to 6 × 10^3 Pa·s in the distal zones (slope < 16°). Partial roofing of the lava channel formed a short-lived lava tube (Fig. 3E). The maximum flow-length was 2.3 km and it covered 20.8 ha of terrain that had not been previously affected by lava (Fig. 1E). This phase was accompanied by the formation of a set of fractures further to the north (Rodríguez-Pascua et al., 2024). The vents formed the day after the highest peak of SO_2 emissions recorded up to that point in the eruption (PEVOLCA, 01/10/2021 (PEVOLCA Scientific Committee Reports, 2021; Ubide et al., 2023)), which was associated with a renewed seismic activity (Oterino et al., 2023). The fumarolic activity to the north of the cone ceased on 4 October, and these distal vents were no longer active. These vents were covered by later lava flows.

4.1.4. Phase 4: 25–26 November

The next set of distal vents formed after 54 days, comparatively late in the eruption. The first vents of this second phase were spotted on 25 November following an increase in the effusion rate of the main eruptive fissure at 9:00 h (PEVOLCA report 25/11/2021, (PEVOLCA Scientific Committee Reports, 2021)) and preceded by a previous increase in seismicity during 12 days (Oterino et al., 2023). An uplift of 4 cm on the terrain was also detected on 18 November on LP03 station and on 25 November (https://www.ign.es/web/ign/portal/vlc-gps). Continuous lava fountain activity with a maximum height of 600 m occurred during this period (Birnbaum et al., 2023).

This phase started with the reactivation of the southern fissure-type vent (V5) located at the highest topographic part of the scoria cone in the SE tip of the main eruptive fissure (Fig. 1E). The issued lava headed southwest arriving at the cemetery of Las Manchas, reaching a total length of 2.7 km and occupying 9.5 ha (Figs. 1E3 and 5A1). This was followed by the burst up of scarce individual vents opened towards the SW located around 965 m a.s.l., being separated by dozens to hundreds of metres in four sets of fissure-type vents aligned ENE-WSW (Fig. 5 A2). At 11:00 (PEVOLCA report 25/11/2021, (PEVOLCA Scientific Committee Reports, 2021)), a fissure with three vents was spotted with effusive activity and spattering activity issuing pāhoehoe lava at the southern crater rim with a NE-SW alignment (EFS 3, Figs. 1E, 5A1 and 5C). A few hours later (14:00–14:20), six scattered vents were spotted at the southern base of the scoria cone, striking ENE-WSW at distances of ~321 m to ~761 m from the main vent (EFS 4 to 6, Figs. 1E2, 5A2, 5B, 5C, 5D, 5E). The day before, at 16:45, a thermal anomaly was observed with RPAs thermal camera in this area. These vents opened in steep slopes and were accompanied by a system of surface fractures separated 20–150 m between the nearby ends and striking NW-SE, N-S and NE-SW (Figs. 1E3, 1G and 4D). In addition, slope failures (with associated landslides and scarps) with displacement of 10–15 m and associated with intense fracturing and listric faults were recorded by RPAs (Fig. 5B and C). The pāhoehoe lavas emitted from these distal vents changed into transitional lava flows and ‘a'ā morphologies with increasing distance from the vents. The lavas covered about 5.5 ha of urban area and destroyed several buildings.

Subsequently, in the evening of 25 November at 17:00 h five additional vents opened between ~1013–1192 m from the main vent (EFS 7, Figs. 1 E3 and 5 A3). These vents opened at 690 m a.s.l. just in front of a house, building a small spatter cone (Fig. 5F), the eruptive fissures measured on field have a mean opening of 20 cm wide. Altogether, a total of twelve vents striking ENE-WSW opened along a 190 m-long lineament (Figs. 1 E3 and 5 A3). These vents emitted very fast degassed pāhoehoe lavas moving at a maximum of 5 m·s^{-1} near the vents and more than 200 m far from the source. The lava fronts moved at apparent speeds of 0.1 m·s^{-1}. The lava flow length from the house reached ~0.8 km. Afterwards in the evening, after 20:00 h, several vents opened ~1602 m from the main vent (at ~600 m a.s.l near a solar power plant) forming a 24-m-long fissure striking NW-SE (EFS 8, Fig. 5A4 and G). The vents opened on gentle slopes (<16°) and exhibited a moderate outflow of pāhoehoe lava of 0.7 km-length and occupied at least 6 ha, covering partially the lava flows of the first event in the morning. These lavas went unnoticed since they covered lava emitted during the morning event. The pāhoehoe lava flows measured in the field at longer distances (>600 m from the source) were up to 1 m thick; not able to enter through the windows of the buildings, usually with a mean value of 0.5 m thickness in intermediate zones and less than 0.4 m near the eruptive fissures. Taking this into account and assuming a constant effusion rate (Jeffreys, 1925), a lava viscosity of between 78, 121 and 486 Pa·s is inferred. Several fractures with an echelon arrangement and graben-like structures (mean opening displacement of 1.5 and 2 m) were observed to the south and following the vent alignment (more details in (Rodríguez-Pascua et al., 2024)), adding up to 49 cracks measured on terrain distributed along ~1500 m. This episode was active at least till 26 November at 08:30 h. The numerous lava flows erupted from this episode covered a surface of 14 ha approximately.

4.1.5. Phase 5: 28 November – 3 December 2021

New vents opened on 28 November following a period of high-effusive activity, characterised by lava emission from the northern crater and channelled beneath the surface through a lava-tube located at the west scoria cone's base (Calvari et al., 2026). On 26 November, deformation around the cone was detected followed on 28 November by a slightly deflation of the surface of 4 cm at LP03 (PEVOLCA report 27/11/2021 (PEVOLCA Scientific Committee Reports, 2021) and IGN). The first sequence starts on 28 November, at 02:40 h, vapour and gas emission anomalies were detected in the southern crater and later on the NE flank of the scoria cone, followed by an increase in the main vent activity. At 03:18 h a fissure opened in the eastern base of the cone striking E-W (Fig. 1 E2), ~163 m from the main fissure, followed by an effusive episode at 03:34 h that opened six vents (EFS 9, Fig. 6A) and start to emit a lava flow. This first vent was dominant with a Strombolian jet and at least five peripheral scattered smaller vents (Fig. 6A and B).

The main fissure vent was active with explosive behaviour emitting ash and gasses (Fig. 6A) at the same time till 05:37 h. At 06:58 h of the 28 November, the explosive activity stopped, being mainly effusive in the new vents. These vents were located at the scar of a partial lateral collapse produced in the first hours in the morning after 03:34 h. The collapse was on the cone flank oriented NE at the northern side of the cone. The scar produced by the event opened the path for seven fissure-type vents (EFS 10–11, Figs. 1E2 and 6C) that were spotted (between 11:40–12:22 h) and aligned N-S (Figs. 1E2 and 1F). Furthermore, during the time-interval, the EFS 10 propagated ~65 m in the same direction N-S, opening another brief path for the magma to the surface (EFS 11, Figs. 1E2 and 6A). The resulting fissure, with a length of ~150–160 m and at least eight distal fissure-type vents, erupted mostly in a Hawaiian effusive-style and with one explosive vent in its upper part that generated phreatomagmatic pulses with 10-s lapses. In addition, an increase of vapour and gas emission at the eastern side of the scoria cone flank was observed. These early formed vents were accompanied by the opening of a N-S striking double vent in the NW (Fig. 1 E2); the distance between the vents being about 5 m (EFS 12, Fig. 6A and D). The lava flows were initially pāhoehoe lava-speeds measured of ~2 m·s^{-1} near vents and ~ 1 m·s^{-1} at distances of ~500 m in the transition to ‘a'ā. During fieldwork, an initial viscosity of 194 Pa·s, with a maximum of 608 Pa·s, has been calculated for these pāhoehoe lava flows. This event formed small-sized hornitos (Fig. 7 C2). The following night the dominant vent (EFS 9) had another lateral collapse at the northern side of the scoria cone and the activity of the peripheral vents became focused on one spot forming an adventive vent and a crater oriented NE-SW (EFS 9 crater Fig. 1 E2).

The next sequence starts on 1 December the activity was focused on

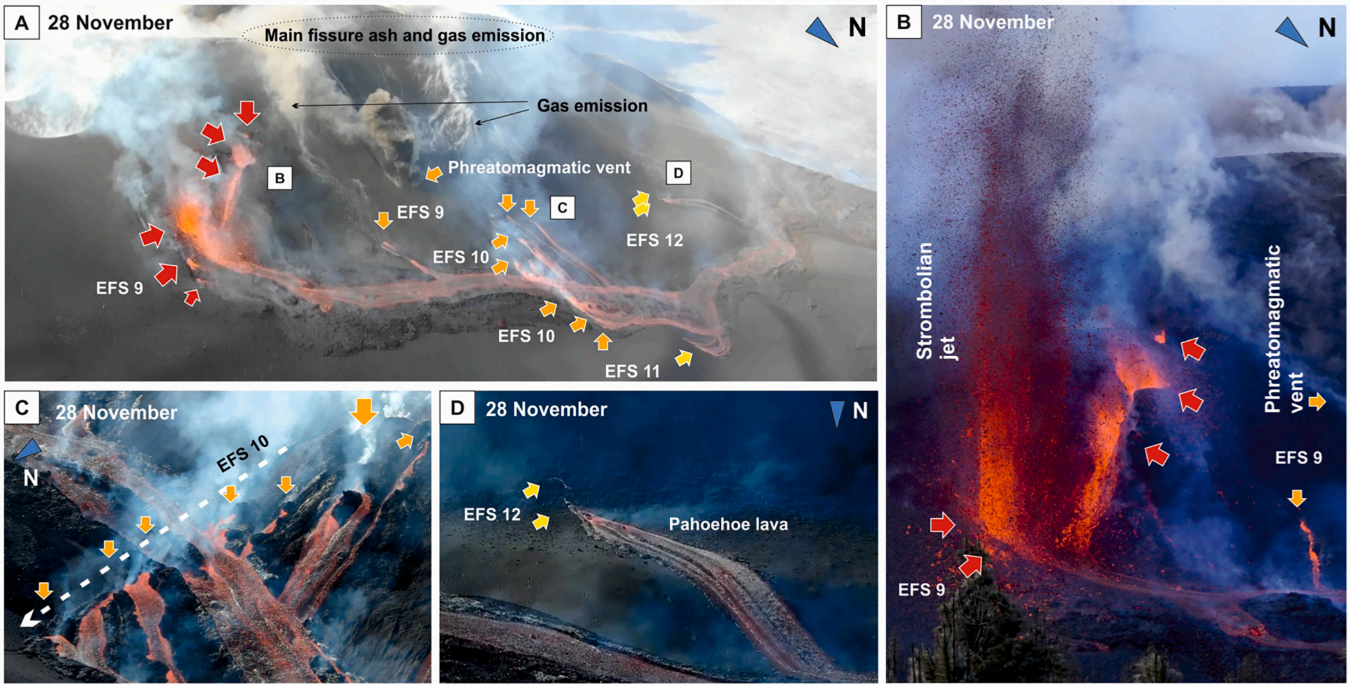

Fig. 6. A) In-field photographs of 1st sequence of the 28 November third stage network of coalescent vents of the main eruptive fissure of the NE with EFS 9 to 12, explosive style is observed with ash and gas emission, gas emission also in the flanks near the vents and phreatomagmatic pulse near EFS 10–11. Red arrows (first hours in the morning): adventive crater vents group (EFS 9) with explosive style and main vent with high-effusive activity; orange arrows (mid-morning): N-S fissure-type vents set (EFS 10–11) with effusive style emitting pāhoehoe-type lavas. Yellow arrows (midday): EFS 10 propagation to the north and double-vent NW of the cone (EFS 12) defining parallel fissures with lava emission N-S trend. B). Detail of EFS 9 on 28 November with the vents that conforms the fissure. C) 28 November, detail of EFS 10–11 fissure with N-S alignment of the vents that conform it. D) Detail of EFS 12 double-vent and pāhoehoe lava flow. The third stage 1st sequence started with the southern vent with a Strombolian behaviour that ended up being dominant over the rest forming an adventive crater in the scoria cone. The activity developed as an intense effusive episode that propagated in December and formed minor lava emission structures like spatter cones and hornitos. (For interpretation of the references to colour in this figure legend, the reader is referred to the web version of this article.)

the adventive crater (EFS 9, Fig. 7A), on EFS 12 and scarce activity on EFS 10–11, forming a spatter cone (Fig. 7 C1). The same day at 14:41 h a fissure-type double-vent was spotted striking N-S (Fig. 1 E2), coinciding with a local fissure slip/fracture trending NW-SE (EFS 13. Fig. 7D). The number of vents increased to 9 following the NW-SE fracture with 2 vents aligned N-S (EFS 14, Fig. 7C and D). In addition, another spatter cone and peripheral hornitos were observed with high-effusive rates and discharging large volumes of pāhoehoe lavas. On 2 December EFS 10–11 were no longer active (on fieldwork hornitos formed by spattering activity remains (Fig. 7 C2)), whereas the EFS 13–14 ended up forming a complex lava tube system with drainages and hornitos aligned (Fig. 7 D1). Fieldwork studies on the hornitos and eruptive fissure has yielded an eruptive fissure mean-opening of 50 cm. Furthermore, new fractures formed at the northern side of the cone affecting buildings and the terrain (Rodríguez-Pascua et al., 2024). This episode coincided with the formation of a graben-like structure (Fig. 5A) at around 15:00 h (Walter et al., 2023) of a maximum width of ~54 m in the southern part of the cone in the “Hoya de Las Plantas” prehistoric crater (Fig. 1 E3). This graben being 54 m wide and 150 m long and striking *NE*-SW. In total 36 fractures have been found related to this episode over a total distance of ~1300 m. The coalescent vents activity that started forming the adventive vent on 28 November ended up forming a well-developed cone with its own crater bonded to the main scoria cone complex. This adventive vent emitted over 138.2 ha of ‘a'ā and blocky-lava-flow morphologies due to partial collapses of the crater, with a maximum flow-length of 4.8 km with decrease of velocities down to 0.02–0.003 $m{\cdot}s^{-1}$. The viscosity from these thick lava flows was about 6.8×10^4 Pa·s. The maximum distance of these eccentric vents between EFS 9 to 13 extends half a kilometre, parallel to the same direction of the main eruptive fissure (NW-SE). The activity of these vents at the last stage gradually decreases until at 07:20 h on 3 December, when just residual activity of the lava flow is observed. Following a period of non-activity, the same day at 17:40 h, the main eruptive fissure reactivated with explosive activity and lava fountaining that can be observed in the southern cone.

4.1.6. *Phase 6: 3–7 December 2021*

On *3 December*, following uplift of 6 cm in Jedey LP03 Station (PEVOLCA 03/12/2021, (PEVOLCA Scientific Committee Reports, 2021)), effusive activity fed a lava flow emission from the southern crater of the main eruptive vent (5.4 ha), reaching 1.2 km. The next day, on 4 December, several vents were spotted ~2180 m from the main vent to the W (Fig. 1 E4), with the formation of a small E-W fissure, that emitted briefly pāhoehoe-lava through two graves in the local cemetery (Fig. 8B) at 540 m a.s.l. (EFS 15, Fig. 8A5). There was little activity in the main vent at 07:00 h. Later, two fissures were identified (8 vents associated, 20 cm mean opening of the eruptive fissures) on a RPAs thermal image (Fig. 8 C1) at around 2310 m from the main vent to the W of Mt. Cogote Holocene cone (EFS 16, Fig. 8A6) trending ENE-WSW. The length of each of the fissure-type vents was around 60 m while the lava flowed up to 50 m from the vents (Fig. 8C). The main vent was active at the southern crater of the scoria cone at 19:15 h. Additionally, a NW-SE 40 m long fissure with five vents (EFS 17, Fig. 8) at a distance of ~2365 m from the main vent opened in a ridge, propagating through the blocky lava emplaced previously on September. The mean field-measured opening of this fissure is 30 cm.

In addition, five fissures with 21 new distal vents were spotted at 11:55 h over 2524 m to 2718 m from the main vent (Fig. 1 E4) in the Todoque urban area (EFS 18, Fig. 8A8). The starting fissure opened at 520 m a.s.l. with NE-SW striking on a wall, producing a fault with a maximum opening of 2 m without lava emission. Consequently, a few metres to the west, a fissure-type vent is located with a brief emission of

(caption on next page)

Fig. 7. In field photographs from the 2nd sequence of the third stage: A) 01 December well-developed adventive crater with EFS 9 at the scoria cone complex with the main eruptive fissure and EFS 10–11 and EFS 12 active. Image from Spanish National Police. B) 01 December spatter cone from EFS 12. C) In field-photographs of later stages of the coalescent third stage of 2 December second phase with a high-developed adventive vent with its own scoria cone developed and spatter cone derived from the EFS 12 and 14 with a hawaiian phase emitting pāhoehoe-type lavas. Blue dotted line marks developed EFS 12 spatter cone -without activity. D) 2 December RPA thermal image of EFS 13 and 14 with fissure-type vents and detail of the fissure slip formed on the cone flank. C1) Spatter cone on 1 December EFS 12 C2) detail of a small-hornito/spatter cone from 2 December EFS 10. D1) Hornitos from 2 December EFS 14 aligned N-S (red dotted arrow). The third stage 2nd phase was characterised by the propagation of fissure-type vents up to the NW through cone fissures, probable related with the cone instability due the pressure-loss of the parallel injected dike. This episode ended up with a meter-size front of blocky-lava that reached more than 3.5 km downslope. (For interpretation of the references to colour in this figure legend, the reader is referred to the web version of this article.)

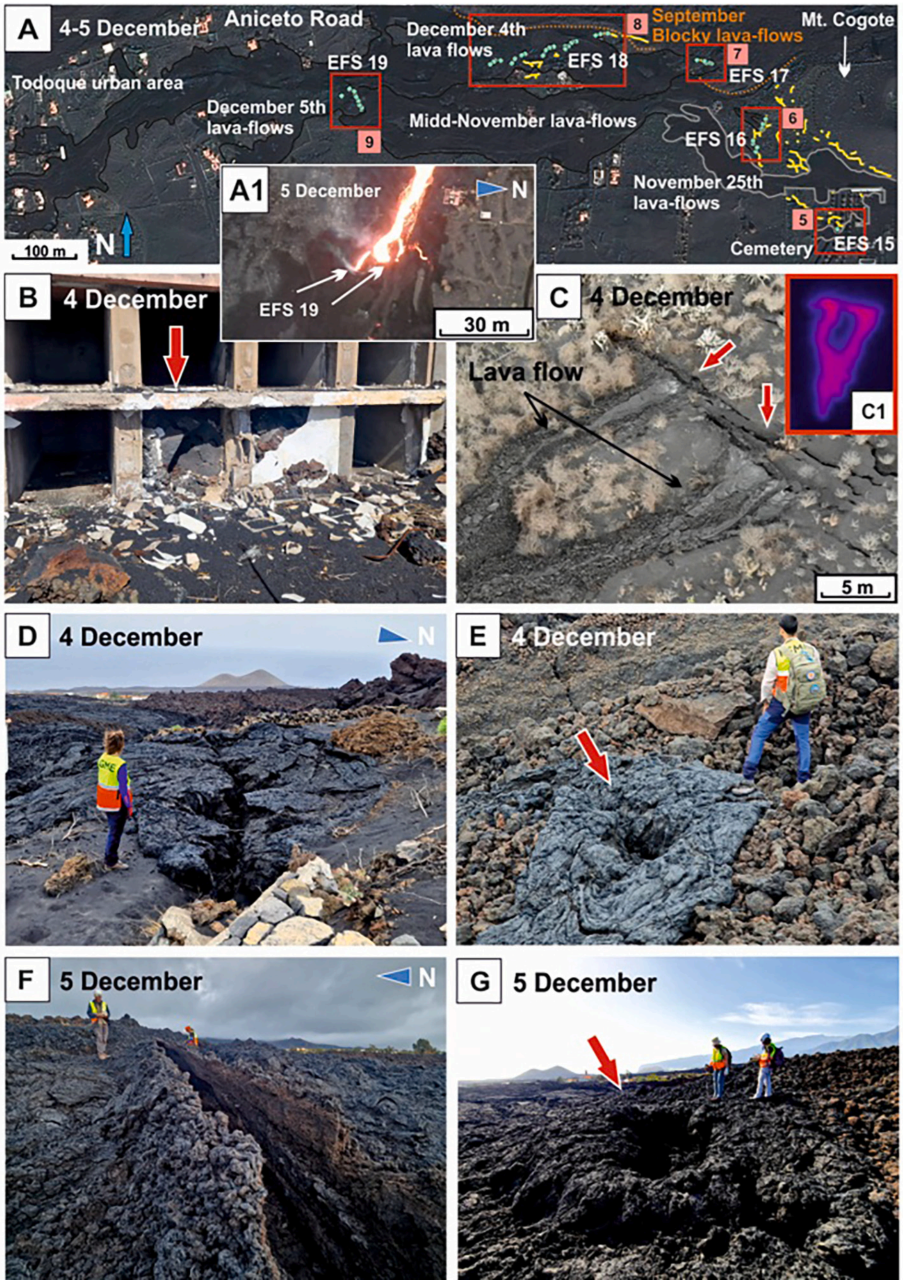

Fig. 8. A) Region at Todoque urban area and W of Mt. Cogote Holocene cone: 5 (EFS 15, cemetery), 6 (EFS 16, Mt. Cogote slope) and 7 (EFS 17, Blocky lava): 4 December morning; 8 (EFS 18, Aniceto Road E): 4 December evening; 9 (EFS 19, Todoque urban area): 4–5 December evening. Orange dotted line represents blocky lava flows from September, black line ‘a'ā flows from mid-November and December lava-flows; A1) RPA image from morning 5 December of EFS 19. Field photographs of distal vents (the persons in the photos provide a scale): B) Cemetery EFS 15 vent opening from a grave. C) RPA image from N-S Cogote Mt. fissure-vents (EFS 16) from the very early 4 December with short-lived lava flows and thermal image (C1) of the lava emission. D) EFS 17 initial fracture and first fissure-type vent opening SW oriented. E) Detail of vent from 4 December EFS 19 with pāhoehoe lava opening through previous ‘a'ā lavas and spattering. F) 5 December EFS 19 vent with drainage connected to a short-lived lava tube. G) EFS 19 with vent-aperture of pāhoehoe lava with spatter in previous ‘a'ā lavas. Photogrammetry images taken from Pléiades1 “© CNES (2021)”, data provided by Distribution Airbus DS and “TICOM soluciones S.L – GRAFCAN – Gobierno de Canarias”- Accessed 12/12/2024. https://tiles.arcgis.com/tiles/hkQNLKNeDVYBjvFE/arcgis/rest/services/dron_fotogrametria_01102021_csic/MapServer

cooled pāhoehoe lava (no activity observed, fissure with 40 cm mean opening) (Fig. 8A). At ~10 m, a second vent is observed with incandescence, cooled pāhoehoe lava and an active lava tube of ~100 m-length to the west (Fig. 8A), and further four non-active vents to the west that break through previous ‘a'ā lava. The activity continued ~75 m further with two vents emitting pāhoehoe lava and several vents with spattering and bubble bursting in the lava channel, defining a total of 193 m-long lineament (Fig. 9A). Many lava tubes and hornitos (Fig. 9A) were formed along the vents alignment in a terrain sloping about ~13°. The lava discharged in this phase from the vents was characterised by a degassed fast-flowing pāhoehoe lava that destroyed more of the residential areas (Fig. 9B). Lava flow speed measured <200 m from the vents reached a velocity of ~3.1 $m \cdot s^{-1}$ near the vents and up to 1.7 $m \cdot s^{-1}$ more than 500 m from the distal vents. Pāhoehoe lava flow front at ~800 m from the vents, observed by drone observations between 12:05 h and 12:36 h, spread 267 m, with an estimated lava front speed of 0.14 $m \cdot s^{-1}$ is estimated (Fig. 9C). At 18:00 h the activity of the main vent increased. There was explosive activity in the central part of the scoria cone and at 19:15 h there was renewed effusive activity with lava fountains in the northern crater. Nearly 8.6 ha of land were covered by lava flows of 1.5 km-length from this episode.

On *5 December* began the final episode of distal vents forming at the surface along the Aniceto Road at 427 m a.s.l. with a fissure spotted at 7:43 h of eleven vents opening at 2944 m from the main vent (Fig. 1 E4) striking NW-SE (EFS 19, Fig. 8 A9) and being 60 m long. Along the fissure, lava tube-drainages (Fig. 8F) and small-sized hornitos with spatter (Fig. 8G) can be found. The lava flows reached 2.7 km till the coast on the same day covering a total of 31.6 ha of surface in less than one hour. Additionally, several cracks and fractures opened up on the south-western flank of Mt. Cogote and in the urban area during this final episode (cf. (Rodríguez-Pascua et al., 2024)), with a complex of 533 cracks related to this episode distributed along ~1600 m. This event of multivent opening formed on generally low gradient slopes (<9°). On 7 December the activity came to an end, with ephemeral vents still active

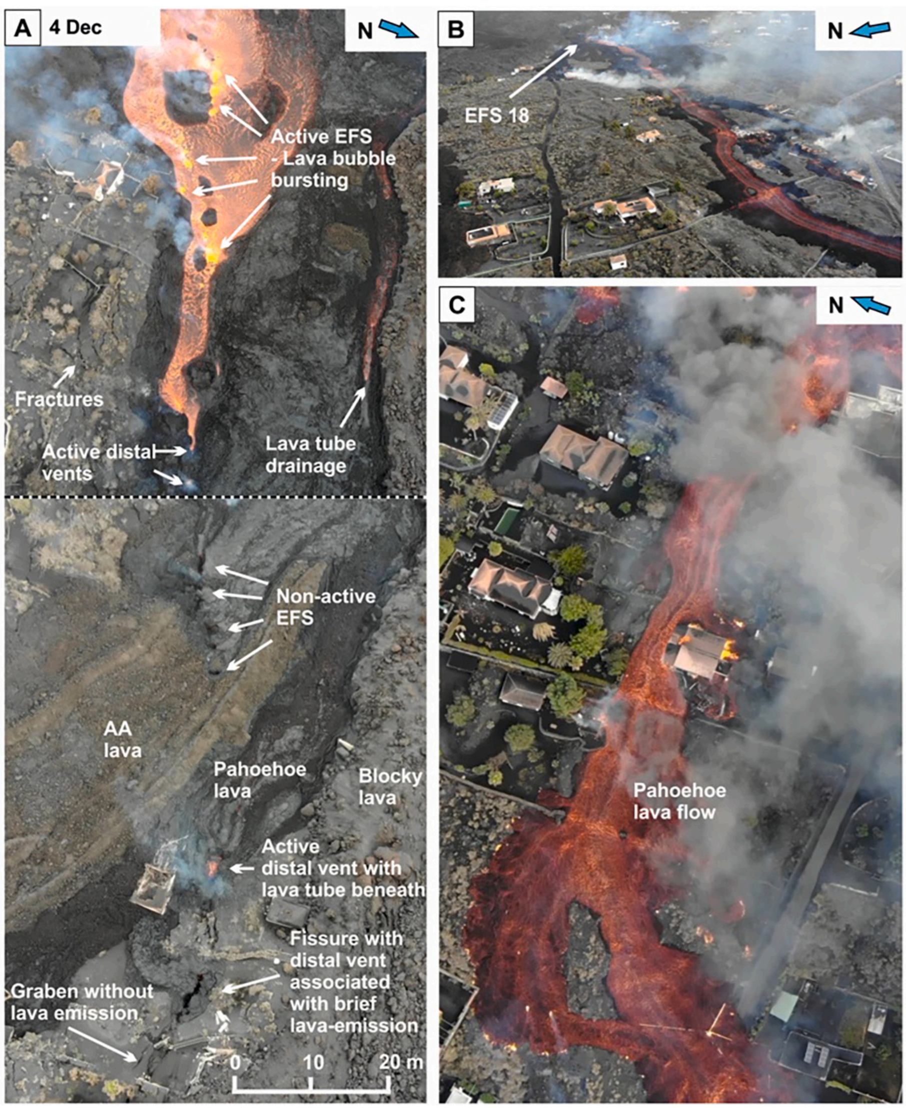

Fig. 9. 4th December: A) 12:35 complete RPA footage of SDV EFS 18 oriented WSW. From the bottom to the top of the image: detail of the fissure-type vents that start at the E with a fissure in the previous terrain without lava emission that propagates to the W and has a first brief emission of pāhoehoe-lava downslope. Three types of lava morphologies can be observed: blocky, ‘a'ā and pāhoehoe, with the last one derived from the distal eruptive vents of the SDV. The fracture continues in the terrain to the E were an active vent can be observed. Further in the middle of the image several non-active vents can be observed aligned breaking through ‘a'ā previous lava-flow. A few metres following up to the E active vents are spotted and a lava tube drainage parallel to the N, probably related to the first vent upslope. Further to the E, in the lava flow, two sets of distal vents alignment appear with bubble bursting and spattering activity. Parallel to this vent-alignment several fractures of the terrain are observed. B) 12:23 RPA images from the EFS 18 location and lava flow invasion. C) 12:25 RPA image with detail of pāhoehoe lava flow spread and damage to buildings.

discharging lava flows. Considering the gentle slopes and brief thickness of the lava flows measured in the field, a viscosity between 70 and 202 Pa·s has been obtained from the lava flows near vents and further (<200 m) and 806–9.7 × 10^3 Pa·s from lava flows at larger distances (500–1000 m) on lava transition from pāhoehoe to ‘a'ā.

5. Discussion

5.1. Opening of vents and hazard implications

The analysis of historical eruptions on La Palma Island (Fig. 2) shows that vents from fissure eruptions can opened at distances of over 4 km from the first eruptive fissure, with vents opening at least in two distinct fissures oriented in different directions. Most of the prehistoric and historic vents are concentrated in the central part of the CVR and along a N-S alignment with eruptive fissures almost 2500 m long. Other modern general studies of spatial analysis of volcanic hazards in La Palma (Martí et al., 2022) suggest that the eruptive fissures account for approximately 76% of the total of fissures on the island with a maximum length of 1640 m.

The multi-vent process of the 2021 eruption started with the opening of six vents of different behaviour that defined a large fissure were the main scoria cone complex developed by the pyroclastic accumulation. The scoria cone, concentrated the effusive activity in the lower elevation crater and the explosive activity in the higher elevation craters (with several paroxysms accompanied by shock waves). The vents associated to the craters showed Hawaiian and Strombolian activities at lower altitudes and phreatomagmatic activity at higher altitude. After 48 h, distal vents, often forming large fissures, were opened far from the main cone. Based on this study, these vents can be classified into three stages according to their date and location: First Stage (EFS 1–2), Second Stage (EFS 3–8 and EFS 15–19) and Third Stage (EFS 9–14) (Fig. 10).

The First Stage has two main phases: (1) the 1st on 20 September and (2) the 2nd phase on 1 October, both of them located in the north-western part of the scoria cone (Fig. 1 E1) less than one kilometre from the main vent. The vents associated with the two eruptive phases opened approximately ten days apart. (Fig. 10). These vents opened following two directions, one to the NW-SE and another *E*-W that EFS 1 and 2. The lavas emitted during this stage covered a total of 47.5 ha of terrain.

The Second Stage occurred in the southern part of the scoria cone and could be grouped by their proximity to the southern craters of the main vent into three phases, separated by ten days (Fig. 10): (1) During the evening 24 - morning 25 November, vents open less than 0.5 km from the main vent, in the southern crater and the base of the scoria cone (Figs. 11A, 5A1 and 5A2) comprising EFS 3 to 6; (2) From the evening of 25 November to the morning of 26 November, between 1 and 2 km from the southern craters, in the El Corazoncillo urban area vents of EFS 7 to 8 were opened (Fig. 11A, Figs. 5A3 and 54A4); Finally, on 4 December, new vents opened in El Corazoncillo urban area (Fig. 11A and Fig. 8 A5-A8) which comprises EFS 15 to 18 and on 5 December on Todoque urbanization (EFS 19) (Fig. 8 A9). The lava emitted during the Second Stage was of low viscosity and degassed, producing a very fast-flowing lavas and covering 50 ha of urban areas such as El Corazoncillo and Todoque in less than an hour. In addition, the hazard increase because the background noise of seismic activity does not make it possible to detect magma propagating to the distal vents. Local inflation of the surface at GNSS LP03 was not enough to detect clearly the event without a constant observation of the area.

During the days preceding the 24 November and 4 December events, there was a fivefold increase in CO_2 emission (compared with background values) in some of the areas were these distal vents appeared (PEVOLCA-25/11/2021 y 03/12/2021 (PEVOLCA Scientific Committee Reports, 2021)). The only confirmed human fatality associated with this eruption occurred several days earlier, on 12 November, as a result of gas intoxication in the same area. In addition, 143 ppm of CO and 17% O_2 were found together and several dead animals detected by the UME in The Corazoncillo urban area (UME Report 231800ZNOV21, Fig. 5). These values eventually decreased to negligible on 26 November, even in confined spaces. Recently, over 5000 ppm of soil-CO_2 gas concentration has been detected in Second Stage system, also ≤8000 HCl and ≤ 12,000 H_2S and temperatures over 60 °C. Moreover, the values of the CO_2 emission after the eruption have been exceeding the 50,000 ppm and 200,000 ppm at La Bombilla and Puerto Naos urban areas respectively (IGN; UME Report 200600ZDIC21; PEVOLCA Report 25/12/2021 (PEVOLCA Scientific Committee Reports, 2021; D'Auria et al., 2023)) with daily variations and levels under 15% of O_2 on air, being worse inside the buildings, sewerages and garages (UME Report 240600ZDIC21 and 080600ZDIC21). (Rodríguez-Pascua et al., 2024) also states a relationship between gas emission/temperatures and the fractures during the eruption.

The Third Stage occurred during the interval between EFS 7–8 and EFS 15–18 (Second Stage). The activity change to the NE flank of the scoria cone (Fig. 10). Two main events can be differentiated: (1) on 28 November (Fig. 6A), characterised by the formation of a new vent that formed a *NE*-SW oriented crater and several fissure-type vents (EFS 9 to 12); (2) between 2-morning 3 December (Fig. 6B) that opened further vents in the northern flank of the scoria cone forming EFS 13 to 14 (Fig. 6C). Lavas issued during this stage covered the largest area, with a total extent of 138 ha.

The background noise in the seismicity and deformation signals prevented the detection of clear precursory signals of distal vents opening. Although volcanic gases were detected in the area, they were not identified as precursors, as the site was already affected by the ash dispersal plume. Greater attention should be paid to such signals during future eruptions. Diffuse degassing surveys should be conducted to distinguish diffuse degassing from the gases derived from the eruptive column. Taking this into account, a sufficiently wide exclusion zone should be considered, taking into account the potential opening of emission centres located at some distance from the main eruptive fissure. In addition, beyond the hazards directly associated with the opening of new vents, these centres commonly issue highly fluid lavas capable of impacting areas several kilometres away from the vent.

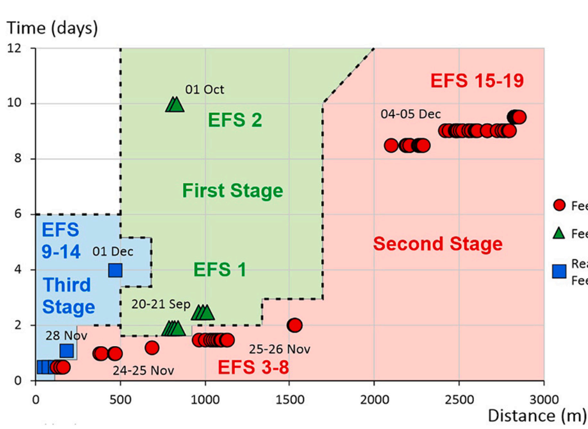

Fig. 10. Plot showing the different stages of distal vent opening in relation to dikes propagation. Green triangles, red circles, and blue squares represent vents related with different stages of feeder-dike emplacement. The days on which the vent were active is also indicated. Distance is measured from the main vent. (For interpretation of the references to colour in this figure legend, the reader is referred to the web version of this article.)

5.2. Analysis of shallow dike propagation and lava flood

The volcanotectonic analysis of the Tajogaite eruption suggests that, during the eruption, at least two feeder-dikes were emplaced, this can be observed on Fig. 10: the *main feeder dike*, striking NW-SE, fed the main

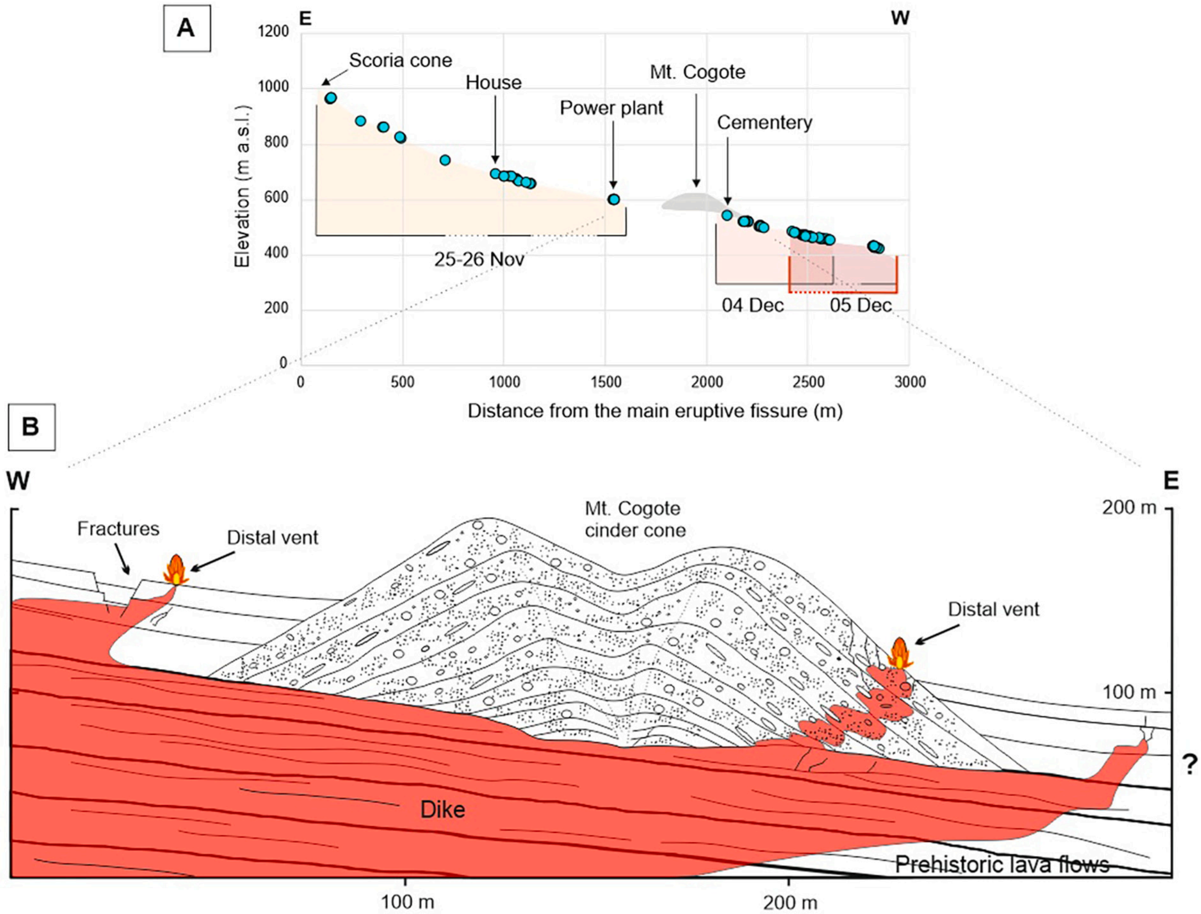

Fig. 11. A) *E*-W plot showing the multi-vent opening process during feeder-dike 2 emplacement as a function of distance from the main eruptive fissure vs elevation in metres and a time-lapse chart with the main map features for reference. B) Hypothetical W-E cross section of Mt. Cogote Holocene scoria (cinder) cone with feeder dike 2 propagation underneath between the 25 November and 4 December. The mechanical properties of the pyroclastic fallout deposit of the scoria cone makes more difficult for the dike to propagate compared with the less ductile prehistoric basaltic lava flow. Fractures and graben-like structures were produced due the shallow intrusion of the dike beneath the surface.

eruptive fissure and supplied magma during the entire eruption (with minor periods of inactivity) and the *secondary feeder dike* (Fig. 11A), which was injected from the main on to the WSW and reached the surface on 24 November. This dike formed segmented eruptive fissures, some of them perpendicular to the direction of intrusion as a result of extensional strain (Rodríguez-Pascua et al., 2026). Several of these fissures were active until 26 November.

The main feeder dike reached the surface of the prehistoric crater of "Hoya de las Plantas" on 19 September, probably propagating parallel to the previous prehistoric feeder dike and gave rise to the main eruptive fissure where the *scoria* cone was built (Fig. 12 A1) and thereby forming a multiple dike (Gudmundsson, 2025). The dike propagated to the WNW and opened four major vents, one being dominant. This vent later merged with the second and third vents to form the main eruptive fissure that propagates to the NW on 20 September (Fig. 12 A2). Ten days later, on 1 October, EFS2 vents opened, suggesting that the feeder dike 1 propagated laterally to the north, following a graben structure NW-SE oriented and creating multiple fracture sets of the previous terrain, this structure was probably formed by the emptying of the dike after reaching the surface. As seen on the image taken by the RPA (Fig. 4D), the surface at the south of the E-W striking vents deflated and produced the first graben-like structure. This structure became more clear in the late 01 October evening, when an additional parallel second graben formed (Fig. 4E). This area was very close to the one where the main vent developed and was more active during the eruption with effusive activity and forming a lava lake. Taking the previous data into account, the inferred speed is approximately 11.9 m/h (285 m/day).

Feeder dike 2 propagated rapidly to the WSW in two main segments (Fig. 11A): the first on 24–25 November (Fig. 12 A3) and the second one 4–5 December (Fig. 12 A5). The eruptive fissure segments were disconnected, being separated laterally by 180 m, and were emplaced 10 days apart. The slope failures with local landslides and fracturing observed during on 24–25 November could be produced by either or both of the following: (1) a very shallow propagation of the feeder dike 2 beneath the surface favoured by a steep slope that changed abruptly along the dike-propagation; or (2) previous discontinuity that acted as a preferred path for the magma to ascent. Feeder dike 2 developed a network of fractures that covered the entire urbanization of El Corazoncillo and Mt. Cogote and had over 65 vents that emerged in close proximity to each other (with a maximum EFS of 18 vents through 350 m of fissure), being the longest-distance dike propagation, reaching nearly 3 km from the main vent. Thus, the inferred dike-propagation velocity is 1.3 m·h^{-1} (30 m·day^{-1}). Moreover, the segmentation of the feeder dike 2 in two pulses suggest that Mt. Cogote played a crucial role in the delay of the propagation of the feeder-dike. The segmentation through two pulses is also suggested by (Przeor et al., 2024), as well as by (De Luca et al., 2022b) who propose an inclined 0.7-m-thick sheet (~1419 m-depth) striking 116° and dipping 62°, and a shallower 1.8-m-thick sheet (~950 m-depth) striking 144° and dipping 64°. The segmentation of the dike was favoured by the presence of the prehistoric scoria cone of Mt. Cogote, that is composed of fallout deposits which is mechanically compliant (soft) compared with the stiffer and more brittle

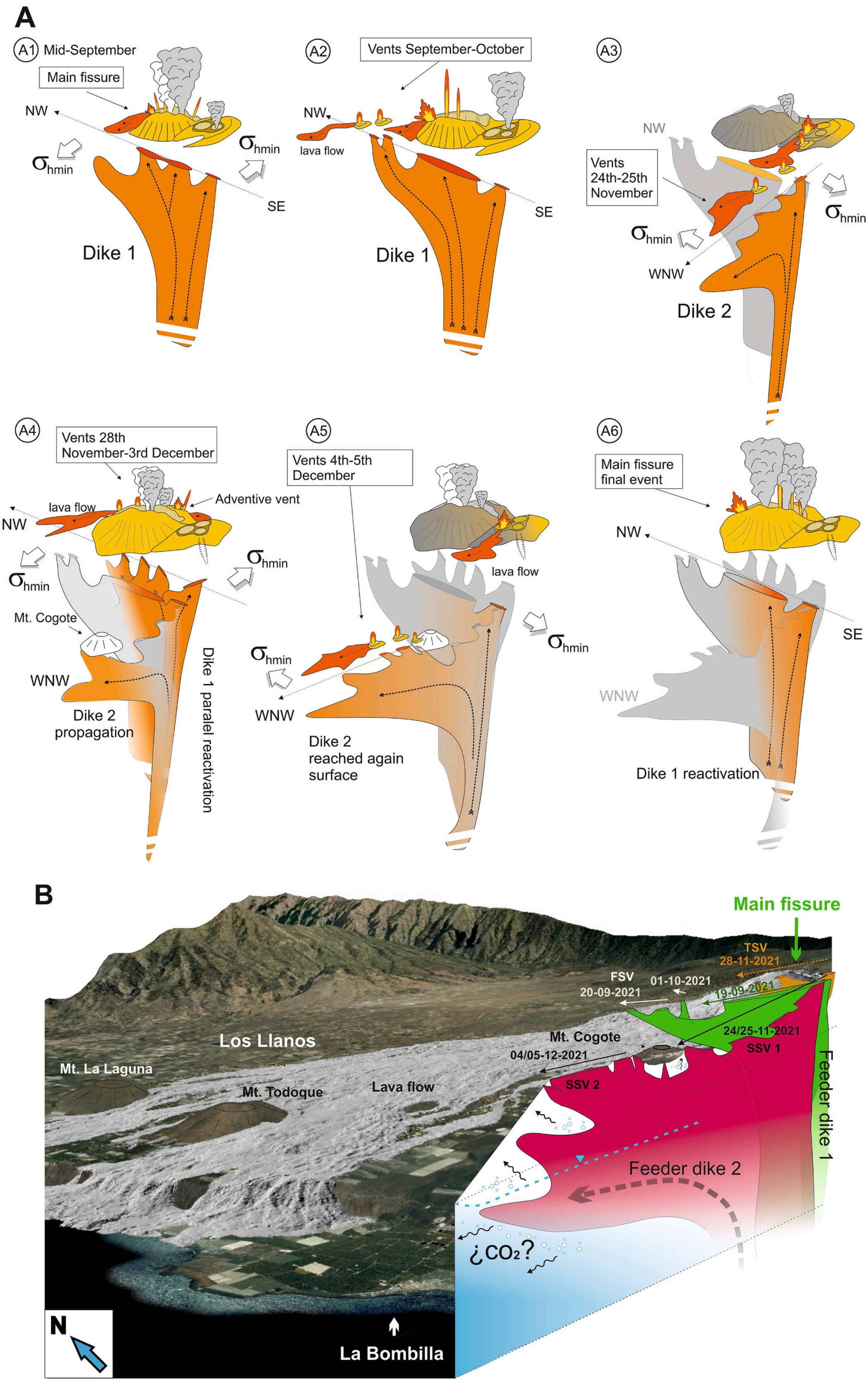

(caption on next page)

Fig. 12. Conceptual model of the dike emplacement. The dike model emphasised the importance of representing the details of the propagation of the dike: A1) Propagation of the main feeder dike (1) trending NW-SE and opening of the sequence of vents that started at 15:12 and propagated to the WNW giving rise to the main eruptive fissure on 19 September. A2) The dike continues its propagation to the WNW opening new fissures on 21 September and 1 October. A3) On 24 November a secondary feeder dike (2) trending E-W began to propagate downslope from the main fissure. A4) The dike 1 reactivates laterally parallel to the main eruptive fissure trending NW-SE and opening fractures and vents locally aligned N-S. A5). Reactivation further to the W of dike 2 that reaches the surface more than 2 km away. A6) After the 5 December the activity concentrates on the main eruptive fissure till the end of the eruption. B) Conceptual model of the feeder dikes beneath the 2021 Tajogaite eruption or Cumbre Vieja Ridge: Dike 1 in green began its propagation on the 19 September and progressed NW-SE on the 21, also the First Stage vents of the 1st October in the N of the main vent. Dike 2 in red that started on the 24 November and continued the direction E-W the 4 December. The activity of the dike 1 continues during the entire eruption, its segments showing high activity for 85 days. The vivid colours represent the predominant activity during that period, grey colour minor activity, less activity, or null activity of the dike segment. Satellite Images and DEM taken from Pléiades1 "© CNES (2021)", Distribution Airbus DS and "TICOM soluciones S.L – GRAFCAN – Gobierno de Canarias", (For interpretation of the references to colour in this figure legend, the reader is referred to the web version of this article.)

lava flows. Thus, the feeder dike 2 emplacement was faster during the 24–25 November (while in the brittle rocks) and slower when approaching the compliant rocks of Mt. Cogote (Fig. 11B). The compliant/soft rocks suppress the tensile stress and have higher material toughness than the brittle lava flows (Gudmundsson, 2011; Gudmundsson, 2020). Hence, the compliant rocks made the dike propagation more difficult, so that fissure opening was delayed until 4 December.

The fast-moving pāhoehoe thin lava veneers that covered the surface from the distal vents of feeder dike 2 and observations during the event, combined with a decrease in lava emission rates (Ubide et al., 2023), suggest a fast propagation of the magma to the surface from the shallow reservoir, possibly following partly an existing discontinuity, a suggestion supported by (Montesinos et al., 2023; Fernández et al., 2022) and (Rodríguez-Pascua et al., 2026). In addition, based on previous works analysing a change in the direction of the hypocentres from NW-SE to ENE-WSW direction (Rodríguez-Pascua et al., 2024), During volcanic unrest and eruption, the local stress field may be substantially modified by dike inflation, magma pressurization or depressurization, edifice loading, topographic gradients, and sector-collapse-related unloading (Passarelli et al., 2015). These processes can locally overprint the regional tectonic stress and redirect dike propagation, vent opening, and volcano-tectonic seismicity. A transient modification of the shallow local stress field, together with pre-existing structural weaknesses, may have favoured the rapid ascent of feeder dike 2 and vent opening. The subsequent fast advance of pāhoehoe lava into new urban areas was then mainly controlled by vent position, effusion rate, lava rheology, lava-channel/tube development, and the local topographic gradient.

On the 28 November (Third Stage) a new segment of the main dike (feeder dike 1) propagated parallel and close to the main eruptive fissure, as indicated by the opening of a network of 23 vents on the northeast flank of the volcano. However, the entire network of vents that opened between the 28 November and 2 December shows a general NW-SE trend. Based on these results, a reactivation of the main feeder dike 1 is inferred (Fig. 12 A4). Apparently, feeder dike 1 was unable to emit lava though vents forming a collinear trend with the existing fissure. The appearance of N-S elongated eruptive vents is consistent with the surface effect, with a NW-SE strike of the feeder-dike being reflected in the overall NW-SE strike of the entire set of eruptive vents formed in this event.

The activity during this period concentrated mainly in the adventive crater with a large Strombolian jet and numerous coalescent vents were active during 5 days, the main vent emitting ash and gases with episodic small phreatomagmatic pulses and the lower EFS showing only effusive activity. The formation of fissure-type vents to the northern part of the *scoria* cone on 2 December at lower altitudes suggests the propagation of feeder dike 1 to the NW of the northeastern flank of the cone with an average velocity of 6.8 m·h^{-1} (164 m·day^{-1}). The graben formed at "Hoya de Las Plantas", a previous crater, also suggests a shallow dike intrusion, in agreement with other results (Walter et al., 2023; Muñoz et al., 2022), producing surface deflation and partial collapses of the adventive crater - which ended up emitting blocky lava with fragments over 5 m-size. However, other studies of this episode (Walter et al., 2023; Muñoz et al., 2022) suggest an oblique dike propagation oriented N-S that produced the adventive vent. These suggestions, however, are primarily supported by remote-sensing results of just one episode (the 28 November SAR amplitude image from COSMO-SkyMed) and the modelling of the 2 December graben-like structure developed during this event. By contrast, our results of the vents alignment observations and 5 day-progression till 2 December with the formation of hornitos-spatter cones and cone-cracks, local landslides and fractures, supports the feeder dike 1 propagating laterally in a NW-SE direction (Fig. 12 A5). Also, for 8 h between 2 and 3 h the activity ceased until the main eruptive fissure began to erupt again (Fig. 12 A6). Taking into account the spatio-temporal variation of the northernmost EFS of the parallel intrusion (EFS 14), on 28 November the propagation velocity of the feeder dike was approximately 25 m·h^{-1} (600 m·day^{-1}).

The appearance of new vents at the northern side of the *scoria* cone at later stages produced the deviation of the lava flow to the northern part whereby the lava flow covered new areas outside the main lava field. However, these newly erupted lava flows were characterised by 'a'ā and blocky morphologies, produced by the constant reshape and reconfiguration of the vents. Pāhoehoe lava morphologies were constrained to the hornitos and spatters of the lower topographic vents and minor in comparison with the total lava flows.

The results of the lava flows from 19 September Phase 1 (feeder dike 1), show an average value of 3.2×10^4 Pa·s of viscosity, they were thick and highly viscous tephrites ('a'ā-type) and similar to the results of (Romero et al., 2022) who estimated the viscosity as 3.9×10^4 Pa·s. The viscosity and thickness of the lava during the first stages of the eruption was very high in comparison with the lava-viscosity at later stages (Ubide et al., 2023; Calvari et al., 2026). In addition to this fact, the lava emitted from the distal vents had lower viscosity, discharging very fast-flowing lava flows (pāhoehoe) that reached mean distances of two kilometres and covered a dozens of hectares' surface in a short amount of time (less than one hour). The results of viscosity inferred in this work from the lava flow velocities on distance from the eccentric vents (Phases 2 to 6), have values below 100 Pa·s with speeds over 2 m·s^{-1} and distances less than 200 m. On detail, phase 6 from 4 December stands out with a lava flow length of almost three kilometres and between 70 and 202 Pa·s in the first 500 m. These low-viscosity values are similar with the ones measured by other studies (Castro and Feisel, 2022; Gisbert et al., 2023) on Tajogaite eruption ranging between 50 and 160 Pa·s and 168–253 Pa·s and only comparable with other volcanoes like Kilauea 2018 eruption with 250–1150 Pa·s. It is noteworthy that the flows emitted from the vents (Second Stage, Figs. 4 and 7) of feeder dike 2 (Phases 2–4 and 6) also had the highest speeds measured on field (3.1 m·s^{-1} and up to 5 m·s^{-1}), similar than the ones measured on 1949 eruption with 10 m·s^{-1} (Klügel et al., 1999).

5.3. Fissure-type vents opening and flank instability

The volcanotectonic structures produced during the eruption, such EFS, fractures, normal faults, slopes failures and a graben, were partly related to the emplacement of the two feeder dikes trending NW-SE and WNW-ESE. Some vents are also aligned N-S, perpendicular to the slope, while the feeding dike is trending ESE-WSW suggesting a local effect close to the surface (Fig. 1F). The formation of the dike-induced structures on during First and Second Stages is consistent with fault-system development (Rodríguez-Pascua et al., 2024) where there are two main faults, the Tazacorte Fault (TZF) and the Mazo Fault (MZF) (Fig. 1C). The NW strike of feeder dike 1 may possibly be related to the Hoya de Las Plantas prehistoric feeder dike creating a multiple dike (Gudmundsson, 2025). The WNW trend is also in harmony with previous eruptions whose fissures show the same alignment and are generally oblique to the slope topography (Day et al., 2000). The eccentric volcanotectonic structures were mainly produced on the flanks of the *scoria* cone of the main eruptive fissure of 2021 eruption during the Third Stage like the graben of 2 December (Fig. 4).

The development of faults in echelon as a result of the movement of the strike-slip faults of Tazacorte and Mazo generated transtensional zones through which magma was able to rise (Rodríguez-Pascua et al., 2026). This fact has been subsequently corroborated by aeromagnetic studies carried out by (Romero-Toribio et al., 2025). This study identifies areas with low magnetic susceptibility associated with magma rise that run parallel to the Mazo and Tazacorte faults. (Fernández et al., 2024) did InSAR analyses of La Palma during the Tajogaite eruption and they were able to observe areas with movement according to the traces of the Mazo and Tazacorte faults. These strike-slip fault systems have remained active for long periods of time previous to the 2021 Tajogaite eruption, at least since 1980 with creep movement, and continue to move today (Rodríguez-Pascua et al., 2024).

We hypothesise that the combination of (1) the weight of the Tajogaite *scoria* cone (with a diameter of 900 m and a height over 180 m), with (2) the substantial uplift produced by the magmatic pulse of the parallel feeder dike intrusion, and the (3) steep previous terrain slope, could have favoured the slope failures. This state suggests that a fissure eruption like this one may encourage, at least locally, volcanic flank instability in large volcanic edifices like CVR. Other volcanic systems such as the Kilauea rift also indicate the interaction between flank-slides and magma systems (Montgomery-Brown and Miklius, 2021). This hypothesis is also supported by previous studies that suggest the possibility of a volcanic flank instability of the CVR induced by the fault system development and shallow intrusions (Rodríguez-Pascua et al., 2024; González, 2022; Rodríguez-Pascua et al., 2026; Day et al., 2000; Rollwage et al., 2024).

5.4. Implications of the subvolcanic structure for post-eruptive diffuse degassing

Lava-flow generated hazards are not only associated with distal-vents opening; anomalous non-visible gas-emission is also a hazard that needs to be taken into account. Concentrations of CO and O_2 detected at localities where the feeder dike 2 later reached the surface and where the fatal gas intoxication occurred, showed an ENE-WSW temporal and spatial progression. The lack of systematic surveys on CO_2 and other gases (CO, H_2S, Rn, etc.) in the area means that accurate information on the temporal and spatial evolution on the gas concentration before, during, and after the feeder dike 2 emplacement is missing.

The continuous *syn*-eruptive high seismicity during the eruption with $M_L > 2$ (Ubide et al., 2023) completely masked the seismic activity corresponding to a secondary dike as this case, and was undistinguishable from the rest of the activity. This may further support the suggestion that the dike used an existing path, like the earlier dike of “Hoya de Las Plantas” volcano, thereby generating a multiple dike. The anomalous gas emission was clearly previous and associated with the propagation of feeder dike 2. When the dike stopped, the gas emission remained active for a while through open fractures. Also, the magma issued by feeder dike 2 was extremely fluid and degassed, taking into account the previous lava flows emitted during the Second Stage from the southern crater, probably large amount of gas was released previously.

The feeder dike 2 propagation from the cone towards east and the subsequent fractures studied by (PEVOLCA Scientific Committee Reports, 2021) suggest that the gas emission during and after the eruption are directly related. This is supported by the results of (Fernández et al., 2022) and (García-Gil et al., 2023a; García-Gil et al., 2023b). The CO_2 became dissolved in an aquifer, saturated it, and was then released towards the surface on the western side of the eruption. Previous works (Montesinos et al., 2023; Fernández et al., 2022) also suggest post-eruptive high-diffuse-CO_2 emission in Puerto Naos and La Bombilla that support our results as to the degassing process being related to the emplacement of feeder dike 2. Nevertheless, degassed magmas also support flank (at lower altitudes) eruptions far from the main vent (Pinel and Jaupart, 2004).

6. Conclusions

Although the geophysical monitoring data did not suggest the possibility of opening new vents far from the main volcanic fissure, studies of historical eruptions at Cumbre Vieja Volcanic Ridge and direct field observations of the 2021 eruption itself demonstrate that distal and eccentric vents can form far from the main vent. Detailed field mapping of Tajogaite volcano shows over a hundred fissure-type vents emitting lava flows over three kilometres away from the main eruptive fissure, commonly at lower altitudes.

These vents were not randomly distributed, but rather clustered and aligned along well-defined volcanotectonic pathways linked to segmented feeder-dike propagation. Particularly, feeder dike 2 propagated westward towards a steep coastal slope and perpendicular to CVR axis. Hence, two circumstances could have facilitated the dike propagation: (1) major strike-slip fault favoured the rapid magma ascent, leading to vent opening along transverse or oblique orientations relative to the main NW–SE trend of feeder dike 1, (2) the favourable topographic gradient likely favoured the shallow dike emplacement.

Subtle surface precursors such as the apparition of fractures, cracks, minor deformation and diffuse degassing were documented prior to vent opening, although they were not recognised in real time as indicators of imminent magma arrival. The analysis of lava flows from distal and eccentric vents shows highly low viscous degassed pāhoehoe lavas that flowed rapidly downslope, invading large urbanised areas without a decrease in the activity at the main eruptive fissure.

Taking into account that the only human death confirmed as a result of the eruption, due to gas intoxication in the same area, occurred days before the emplacement of feeder dike 2 (12 November), daily zonation map-based-monitoring of gas hazards in the exclusion areas should be considered for future eruptions.

Late-stage distal lava flows discharge was sustained by lava-tube drainage and network emptying rather than direct magma supply from depth. The associated development of echelon fractures, normal faults and local graben volcanotectonic structures are compatible both with the effects of transtensional stress conditions and shallow dike intrusion, consistent with historical eruptions at La Palma and analogous basaltic volcanic systems worldwide.

Episodes of slope failure during the Second and Third Stages further highlight transient instability of the eruptive edifice and host rocks, while post-eruptive degassing in coastal areas such as Puerto Naos and La Bombilla is likely linked to permeability enhancement caused by feeder dike 2 propagation. These observations underline the need to explicitly consider distal vent formation in future hazard assessments, incorporating detailed field surveillance, local deformation monitoring, diffuse gas measurements and continuous expert visual observations, potentially supported by drone-based technologies.

CRediT authorship contribution statement

David Sanz-Mangas: Writing – review & editing, Writing – original draft, Visualization, Supervision, Project administration, Methodology, Investigation, Formal analysis, Data curation, Conceptualization. **Inés Galindo:** Writing – review & editing, Supervision, Resources, Project administration, Funding acquisition, Formal analysis. **Agust Gudmundsson:** Writing – review & editing, Writing – original draft, Validation, Supervision, Investigation, Conceptualization. **Raúl Pérez-López:** Writing – review & editing, Writing – original draft, Visualization, Validation, Methodology, Investigation, Formal analysis, Data curation, Conceptualization. **Miguel Ángel Rodríguez-Pascua:** Writing – review & editing, Validation, Resources, Investigation, Formal analysis, Data curation. **Rayco Marrero:** Writing – review & editing, Resources, Investigation, Data curation, Conceptualization. **María Ángeles Perucha:** Writing – review & editing, Resources, Investigation, Conceptualization. **Juan Carlos García-Davalillo:** Writing – review & editing, Visualization, Software, Resources, Data curation. **Juana Vegas:** Writing – review & editing, Visualization, Project administration, Investigation, Funding acquisition, Formal analysis. **Nieves Sánchez:** Writing – review & editing, Validation, Supervision, Funding acquisition, Data curation.

Author agreement statement

We the undersigned declare that this manuscript is original, has not been published before and is not currently being considered for publication elsewhere.

We confirm that the manuscript has been read and approved by all named authors and that there are no other persons who satisfied the criteria for authorship but are not listed. We further confirm that the order of authors listed in the manuscript has been approved by all of us.

We understand that the Corresponding Author is the sole contact for the Editorial process. He/she is responsible for communicating with the other authors about progress, submissions of revisions and final approval of proofs.

Declaration of competing interest

The authors declare that they have no known competing financial interests or personal relationships that could have appeared to influence the work reported in this paper.

Acknowledgements

We thank Gonzalo Lozano from the IGME-CSIC for its support for this work. Special thanks to Eumenio Ancochea and Álvaro Márquez from the Faculty of Geological Sciences of the Complutense University of Madrid for their valuable observations, advice and comments in the work. Also, we want to express our gratitude to Juana Medina Santana and Enrique Sánchez Déniz from “Grupo de Emergencias y Salvamento” (GES) from Government of Canary Islands, and STA from IGME-CSIC, for the RPAs media. The authors are grateful to the reviewers F. Mazzarini and M.G. Gómez-Vasconcelos for their constructive comments, which helped to improve the clarity of our manuscript. This research was funded by the Spanish National Research Council (CSIC) (CSIC-LA PALMA-12- 20223PAL002) and by the Government of the Canary Islands and the Spanish Ministry of Ecological Transition and Demographic Challenge (227G0165-GEOPALMA).

ESRI© ArcGIS pro-2.6.0 (ESRI) software has been used in order to elaborate the cartography and accurately locate and organise the distal eruptive vents located due to fieldwork and UAV photogrammetry images. Pix4D © SA, v.4.5.6 Mapper software has also been used for RPAs image-processing.

Appendix A. Supplementary data

Supplementary data to this article can be found online at https://doi.org/10.1016/j.jvolgeores.2026.108664.

Data availability

The data used is available on the manuscript and links attached on it. Drone videos and images are available in the IGME-CSIC website; original media can be shared upon formal request

References

Andronico, D., Branca, S., Calvari, S., Burton, M., Caltabiano, T., Corsaro, R.A., Del Carlo, P., Garfì, G., Lodato, L., Miraglia, L., Mure, F., Neri, M., Pecora, E., Pompilio, M., Salerno, G., Spampinato, L., 2005. A multi-disciplinary study of the 2002–03 Etna eruption: insights into a complex plumbing system. Bull. Volcanol. 67, 314–330. https://doi.org/10.1007/s00445-004-0372-8.

Becerril, L., Galindo, I., Gudmundsson, A., Morales, J.M., 2013. Depth of origin and overpressure of magma in feeder dikes in El Hierro (Canary Islands). Sci. Rep. 3, 2762. https://doi.org/10.1038/srep02762.

Birnbaum, J., Lev, E., Hernandez, P.A., Barrancos, J., Padilla, G.D., Asensio-Ramos, M., Calvo, D., Rodríguez, F., Pérez, N.M., D'Auria, L., Calvari, S., 2023. Temporal variability of explosive activity at Tajogaite volcano, Cumbre Vieja (Canary Islands), 2021 eruption from ground-based infrared photography and videography. Front. Earth Sci. 11. https://doi.org/10.3389/feart.2023.11934.

Bonadonna, C., Pistolesi, M., Biass, M., Voloschina, M., Romero, J., Coppola, D., Folch, A., D'Auria, L., Martin-Lorenzo, A., Domínguez, L., Pastore, C., Reyes Hardy, M.-P., Rodríguez, F., 2022. Physical characterization of long-lasting hybrid eruptions: the 2021 Tajogaite eruption of Cumbre Vieja (La Palma, Canary Islands). J. Geophys. Res. Solid Earth 127. https://doi.org/10.1029/2022JB025302.

Booth, B., Self, S., Guest, J.E., Skelhorn, R.R., 1973. Mount Etna and the 1971 eruption - Rheological features of the 1971 Mount Etna lavas. Philos. Trans. A Math. Phys. Eng. Sci. 274 (1238), 99–106. https://doi.org/10.1098/rsta.1973.0029.

Calvari, S., 2019. Understanding lava flow morphologies and structures for hazard assessment. Ann. Geophys. https://doi.org/10.4401/ag-8048.

Calvari, S., Ganci, G., Galindo, I., Sanz-Mangas, D., Morgavi, D., Fernández Lorenzo, O., 2026. Emplacement and growth of a stacked tube-fed lava flow field: the 2021 Tajogaite eruption (La Palma, Canary Islands, Spain). Bull. Volcanol. https://doi.org/10.1007/s00445-025-01925-x.

Carracedo, J.C., Troll, V.R., 2016. The Geology of the Canary Islands. Elsevier. https://doi.org/10.1016/C2015-0-04268-X.

Carracedo, J.C., Badiola, E.R., Guillou, H., de la Nuez, J., Torrado, F.J. Pérez, 2001. Geology and volcanology of La Palma and El Hierro, western Canaries. Estud. Geol. 57, 175–273. https://hal.science/hal-03323419v1.

Castro, J.M., Feisel, Y., 2022. Eruption of ultralow-viscosity basanite magma at Cumbre Vieja, La Palma, Canary Islands. Nat. Commun. 13, 3174. https://doi.org/10.1038/s41467-022-30905-4.

Chevrel, O., Harris, A., 2025. Monitoring lava flows. In: Modern Volcano Monitoring. Springer, pp. 295–324, 2025, advances in Volcanology, 978-3-031-86840-5. https://doi.org/10.1007/978-3-031-86841-2_10.

D'Auria, L., Santos, A., Hernández, P.A., Melián, G.V., Álvarez Díaz, A.J., Asensio-Ramos, M., González Pérez, A.M., Pérez, N.M., 2023. Modeling outdoor dispersion of CO_2 at Puerto Naos (La Palma, Canary Islands). EGU Gen. Assem. 2023. https://doi.org/10.5194/egusphere-egu23-3834.

Day, S.J., Carracedo, J.C., Guillou, H., Gravestock, P., 2000. Comparison and cross-checking of historical, archaeological and geological evidence for the location and type of historical eruptions of oceanic island volcanoes. Geol. Soc. Lond. Spec. Publ. 171, 281–306. https://doi.org/10.1144/GSL.SP.2000.171.01.21.

De Luca, C., Valerio, E., Giudicepietro, F., Macedonio, G., Casu, F., Lanari, R., 2022. Pre- and co-eruptive analysis of the September 2021 eruption at Cumbre Vieja volcano (La Palma, Canary Islands) through DInSAR measurements and analytical modeling. Geophys. Res. Lett. 49. https://doi.org/10.1029/2021GL097293.

Ducrocq, C., Árnadóttir, T., Jónsson, P. Einarsson S., Drouin, V., Geirsson, H., Hjartardóttir, A.R., 2024. Widespread fracture movements during a volcano-tectonic unrest: the Reykjanes Peninsula, Iceland. Bull. Volcanol. 86, 14. https://doi.org/10.1007/s00445-023-01699-0.

Fernández, J., Escayo, J., Camacho, A.G., Palano, M., Prieto, J.F., Hu, Z., Samsonov, S.V., Tiampo, K.F., Ancochea, E., 2022. Shallow magmatic intrusion evolution below La Palma before and during the 2021 eruption. Sci. Rep. 12, 20257. https://doi.org/10.1038/s41598-022-23998-w.

Fernández, J., Escayo, J., Prieto, J.F., Tiampo, K.F., Camacho, A.G., Ancochea, E., 2024. Volcanic unrest after the 2021 eruption of La Palma. Geophys. Res. Lett. 51 (11). https://doi.org/10.1029/2024gl108803.

Galindo, I., Gudmundsson, A., 2012. Basaltic feeder dikes in rift zones: geometry, emplacement, and effusion rates. Nat. Hazards Earth Syst. Sci. 12, 3683–3700. https://doi.org/10.5194/nhess-12-3683-2012.

García-Gil, A., Jimenez, J., Gasco Cavero, S., Marazuela, M.A., Baquedano, C., Martínez-León, J., Cruz-Pérez, N., Laspidou, C., Santamarta, J.C., 2023a. Effects of the 2021 La Palma volcanic eruption on groundwater resources (part I): hydraulic impacts. Groundw. Sustain. Dev. 23, 100989. https://doi.org/10.1016/j.gsd.2023.100989.

García-Gil, A., Jimenez, J., Gasco Cavero, S., Marazuela, M.A., Baquedano, C., Martínez-León, J., Cruz-Pérez, N., Laspidou, C., Santamarta, J.C., 2023b. Effects of the 2021 La Palma volcanic eruption on groundwater resources (part II): hydrochemical impacts. Groundw. Sustain. Dev. 23, 100992. https://doi.org/10.1016/j.gsd.2023.100992.

Gisbert, G., Troll, V.R., Day, J.M.D., Geiger, H., Perez-Torrado, F.J., Aulinas, M., Deegan, F.M., Albert, H., Carracedo, J.C., 2023. Reported ultra-low lava viscosities from the 2021 La Palma eruption are potentially biased. Nat. Commun. 14, 6453. https://doi.org/10.1038/s41467-023-42022-x.

González, P.J., 2022. Volcano-tectonic control of Cumbre Vieja. Science 375, 1348–1349. https://doi.org/10.1126/science.abn5148.
Gudmundsson, A., 2011. Rock Fractures in Geological Processes. Cambridge University Press. https://doi.org/10.1017/CBO9780511975684.
Gudmundsson, A., 2020. Volcanotectonics: Understanding the Structure, Deformation and Dynamics of Volcanoes. Cambridge University Press. https://doi.org/10.1017/9781139176217.
Gudmundsson, A., 2022. The propagation paths of fluid-driven fractures in layered and faulted rocks. Geol. Mag. 159, 1978–2001. https://doi.org/10.1017/S0016756822000826.
Gudmundsson, A., 2025. Multiple dikes make eruptions easy. J. Volcanol. Geotherm. Res. 460. https://doi.org/10.1016/j.jvolgeores.2025.108284.
Harris, A.J.L., Dehn, J., Calvari, S., 2007. Lava effusion rate definition and measurement: a review. Bull. Volcanol. 70, 1–22. https://doi.org/10.1007/s00445-007-0120-y.
Hernandez-Pacheco, A., Valls, M.C., 1982. The historic eruptions of La Palma Island (Canaries). In: Arquipélago. Série Ciências da Natureza, 3, pp. 83–94. http://hdl.handle.net/10400.3/4915.
Hjartardóttir, Á.R., Dürig, T., Parks, M.M., Drouin, V., Eyjólfsson, V., Reynolds, H., Einarsson, P., Jensen, E.H., Óskarsson, B.V., Belart, J.M., Ruch, J., Gies, N.B., Pedersen, G.B., 2023. Pre-existing fractures and eruptive vent openings during the 2021 Fagradalsfjall eruption, Iceland. Bull. Volcanol. 85, 1–14. https://doi.org/10.1007/s00445-023-01670-z.
Jeffreys, H., 1925. The flow of water in an inclined channel of rectangular section. Philos. Mag. 49 (293), 793–807. https://doi.org/10.1080/14786442508634662.
Jenkins, S.F., Day, S.J., Faria, B.E., Fonseca, J.F.B.D., 2017. Damage from lava flows: insights from the 2014–2015 eruption of Fogo, Cape Verde. J. Appl. Volcanol. 6, 1–17. https://doi.org/10.1186/s13617-017-0057-6.
Jiménez, J., Gasco Cavero, S., Marazuela, M.Á., Baquedano, C., Laspidou, C., Santamarta, J.C., García-Gil, A., 2024. Effects of the 2021 La Palma volcanic eruption on groundwater hydrochemistry. Sci. Total Environ. 929, 172594. https://doi.org/10.1016/j.scitotenv.2024.172594.
Klügel, A., Hansteen, T.H., Schmincke, H.-U., 1997. Rates of magma ascent and depths of magma reservoirs beneath La Palma (Canary Islands). Terra Nova 9, 117–121. https://doi.org/10.1046/j.1365-3121.1997.d01-15.x.
Klügel, A., Schmincke, H.-U., White, J.D.L., Hoernle, K.A., 1999. Chronology and volcanology of the 1949 multi-vent rift-zone eruption on La Palma. J. Volcanol. Geotherm. Res. 94, 267–282. https://doi.org/10.1016/S0377-0273(99)00107-9.
Lerner, G.A., Siebe, C., Ramírez-Uribe, I., Fisher, C.T., 2024. Temporal and morphological eruption characteristics of lava flows from the Holocene La Taza monogenetic cone. Volcanica 7, 587–606. https://doi.org/10.30909/vol.07.02.587606.
Longpré, M.A., Felpeto, A., 2021. Historical volcanism in the Canary Islands. J. Volcanol. Geotherm. Res. 419, 10736. https://doi.org/10.1016/j.jvolgeores.2021.107363.
Martí, J., Becerril, L., Rodriguez, A., 2022. How long-term hazard assessment may help to anticipate volcanic eruptions: the case of La Palma eruption 2021. J. Volcanol. Geotherm. Res. 431, 107669.
Meredith, E.S., Jenkins, S.F., Hayes, J.L., Deligne, N., Lallemant, D., Patrick, M., Neal, C., 2022. Damage assessment for the 2018 lower East Rift Zone lava flows of Kīlauea volcano. Bull. Volcanol. 84, 65. https://doi.org/10.1007/s00445-022-01568-2.
Montesinos, F.G., Sainz-Maza, S., Gómez-Ortiz, D., Arnoso, J., Blanco-Montenegro, I., Benavent, M., Vélez, E., Sánchez, N., Martín-Crespo, T., 2023. Insights into the magmatic feeding system of the 2021 eruption at Cumbre Vieja inferred from gravity data modeling. Remote Sens. 15, 1936. https://doi.org/10.3390/rs15071936.
Montgomery-Brown, E.K., Miklius, A., 2021. Periodic dike intrusions at Kīlauea volcano, Hawai'i. Geology 49, 397–401. https://doi.org/10.1130/G47970.1.
Moore, H.J., 1987. Preliminary estimates of the rheological properties of 1984 Mauna Loa lava. U.S. Geol. Surv. Prof. Pap. 1350, 1569–1588.
Muñoz, V., Walter, T.R., Zorn, E.U., Shevchenko, A.V., González, P.J., Reale, D., Sansosti, E., 2022. Satellite Radar and Camera Time Series Reveal transition from Aligned to distributed Crater Arrangement during the 2021 Eruption of Cumbre Vieja, La Palma (Spain). Remote Sens. 14 (23), 6168. https://doi.org/10.3390/rs14236168.
Oterino, B.B., Alvarado, G.E., Marchamalo, M., Rejas, J.G., Murphy, P., Franco, R., Castro, D., Garcia-Lanchares, C., Sanchez, J., 2023. Temporal and spatial evolution of the 2021 eruption in the Tajogaite volcano (Cumbre Vieja rift zone, La Palma, Canary Islands) from geophysical and geodetic parameter analyses. Nat. Hazards 118 (3), 2245–2284. https://doi.org/10.1007/s11069-023-06090-y.
Passarelli, L., Rivalta, E., Cesca, S., Aoki, Y., 2015. Stress changes, focal mechanisms, and earthquake scaling laws for the 2000 dike at Miyakejima (Japan). J. Geophys. Res. Solid Earth 120, 4130–4145. https://doi.org/10.1002/2014JB011504.
PEVOLCA Scientific Committee Reports, 2021. Actualización de la Actividad Volcánica en Cumbre Vieja (La Palma). Available from. https://www.gobiernodecanarias.org/infovolcanlapalma/pevolca/.
Pinel, V., Jaupart, C., 2004. Likelihood of basaltic eruptions as a function of volatile content and volcanic edifice size. J. Volcanol. Geotherm. Res. 137 (1–3), 201–217. https://doi.org/10.1016/j.jvolgeores.2004.05.010.
Przeor, M., Castaldo, R., D'Auria, L., Pepe, A., Pepe, S., Sagiya, T., Solaro, G., Tizzani, P., Martínez, J.B., Pérez, N., 2024. Geodetic imaging of magma ascent through a bent and twisted dike during the Tajogaite eruption of 2021. Sci. Rep. 14, 212. https://doi.org/10.1038/s41598-023-50982-9.
Rodríguez-Pascua, M.Á., Perez-Lopez, R., Perucha, M.Á., Sánchez, N., López-Gutierrez, J., Mediato, J.F., Sanz-Mangas, D., Lozano, G., Galindo, I., García-Davalillo, J.C., Lorenzo Carnicero, C., Béjar, M., 2024. Active faults, kinematics and seismotectonic evolution during Tajogaite eruption 2021. Appl. Sci. 14, 2745. https://doi.org/10.3390/app14072745.
Rodríguez-Pascua, M.A., Pedrosa-González, M.T., Perucha, M.A., Sánchez, N., Sáez-Gabarrón, L., López-Gutiérrez, J., Pérez-López, R., Sanz-Mangas, D., Galindo, I., 2026. Emergency intervention for the early estimation of slow creep motion on the active faults of La Palma (Canary Islands, Spain). Nat. Hazards 122, 55. https://doi.org/10.1007/s11069-025-07872-2.
Rollwage, L., Sánchez-Guillamón, O., Sippl, C., León, R., Vázquez, J.T., Urlaub, M., Gross, F., Böttner, C., Krastel, S., Geersen, J., 2024. Geomorphological evidence for volcano-tectonic deformation along the unstable western flank of Cumbre Vieja volcano. Geomorphology 465, 109401. https://doi.org/10.1016/j.geomorph.2024.109401.
Romero, C., 1991. Las manifestaciones volcánicas históricas del archipiélago Canario. Tomo I. Gobierno de Canarias, Consejería de Política Territorial, El Cedro, S.L., p. 695. ISBN: 84-7756-219-9.
Romero, C., Beltrán, E., 2015. El impacto de las coladas de 1706 en la ciudad de Garachico (Tenerife, Islas Canarias, España). Investig. Geogr. 63, 99–115. https://doi.org/10.14198/INGEO2015.63.07.
Romero, J.E., Burton, M., Cáceres, F., Taddeucci, J., Civico, R., Ricci, T., Pankhurst, M.J., Hernández, P.A., Bonadonna, C., Llewellin, E.W., Pistolesi, M., Polacci, M., Solana, C., D'auria, L., Arzilli, F., Andronico, D., Rodríguez, F., Asensio-Ramos, M., Martín-Lorenzo, A., Hayer, C., Scarlato, P., Perez, M., 2022. The initial phase of the 2021 Cumbre Vieja ridge eruption (Canary Islands): products and dynamics controlling edifice growth and collapse. J. Volcanol. Geotherm. Res. 431. https://doi.org/10.1016/j.jvolgeores.2022.107642. Article 107642.
Romero-Toribio, M.C., Martín-Hernández, F., Ledo, J., 2025. High-resolution drone-based aeromagnetic survey at the Tajogaite Volcano (La Palma, Canary Islands): insights into its early post-eruptive shallow structure. Remote Sens. 17 (18), 3153. https://doi.org/10.3390/rs17183153.
Sanz-Mangas, D., Ancochea, E., Huertas, M.J., Herrera, R., Márquez, A., Coello-Bravo, J. J., Ubide, T., 2024a. Mineral assemblage of lavas from the 2021 Tajogaite eruption at La Palma Island. Geo-Temas 20, 1031–1034 (ISSN: 2792-2308).
Sanz-Mangas, D., Galindo, I., Pérez-López, R., Rodríguez-Pascua, M.Á., Perucha, M.Á., Camuñas, C., López-Gutierrez, J., García López-Davalillo, J.C., Lorenzo, C., Lozano, G., Vegas, J., Marrero, R., Hernández, M., Mediato, J.F., Sánchez, N., 2024b. Fissure-type vents at 2021 Cumbre Vieja volcanic eruption. In: EGU General Assembly 2024, Vienna, Austria, 14–19 Apr 2024. https://doi.org/10.5194/egusphere-egu24-2645. EGU24-2645.
Sigmundsson, F., Parks, M., Geirsson, H., Hooper, A., Drouin, V., Vogfjörd, K.S., Ófeigsson, B.G., Greiner, S.H.M., Yang, Y., Lanzi, C., De Pascale, G.P., Jónsdóttir, K., Hreinsdóttir, S., Tolpekin, V., Friðriksdóttir, H.M., Einarsson, P., Barsotti, S., 2024. Fracturing and tectonic stress drive ultrarapid magma flow into dikes. Science 383 (6688), 1228–1235. https://doi.org/10.1126/science.adn2838.
Smith, I., Németh, K., 2017. Source to surface model of Monogenetic Volcanism: a critical review. Geol. Soc. Lond., Spec. Publ. 446, 1–28. https://doi.org/10.1144/SP446.14.
Ubide, T., Márquez, A., Ancochea, E., Huertas, M.J., Herrera, R., Coello-Bravo, J.J., Sanz-Mangas, D., Mulder, J., MacDonald, A., Galindo, I., 2023. Discrete magma injections drive the 2021 La Palma eruption. Sci. Adv. 9 (27), eadg4813. https://doi.org/10.1126/sciadv.adg4813.
Viveiros, F., Silva, C., 2024. Hazardous volcanic CO2 diffuse degassing areas - a systematic review on environmental impacts, health, and mitigation strategies. iScience 27 (10), 110990. https://doi.org/10.1016/j.isci.2024.110990.
Walker, G.P.L., 1971. Compound and simple lava flows and flood basalts. Bull. Volcanol. 35 (2), 579–590. https://doi.org/10.1007/BF02596829.
Walter, T.R., Zorn, E.U., González, P.J., Sansosti, E., Muñoz, V., Shevchenko, A.V., Plank, S.M., Reale, D., Richter, N., 2023. Late complex tensile fracturing interacts with topography at Cumbre Vieja, La Palma. Volcanica 6 (1), 1–17. https://doi.org/10.30909/vol.06.01.0117.
Zanon, V., D'Auria, L., Schiavi, F., Cyrzan, K., Pankhurst, M.J., 2024. Toward a near real-time magma ascent monitoring by combined fluid inclusion barometry and ongoing seismicity. Sci. Adv. 10 (6), eadi4300. https://doi.org/10.1126/sciadv.adi4300.